

Facile wet chemical synthesis and characterization of zinc doped gadolinium oxide nanoparticles for enhanced photodegradation of Rhodamine B dye under illumination of UV light

Leena Vinolia Thaninki^{a,b}; Samson Nesaraj Arputharaj^{*a,c}; Arunkumar Manasai^a

a) Department of Applied Chemistry, Karunya Institute of Technology and Sciences (Deemed to be University), Karunya Nagar, Coimbatore - 641114, Tamil Nadu, India.

b) Department of Chemistry, CMR Technical Campus, Kandlakoya, Hyderabad – 501 401, Telengana, India.

c) Department of Chemistry, Kalasalingam Academy of Research and Education (Deemed to be University), Krishnankoil – 626126, Tamil Nadu, India.

Received 31 December 2021; received in revised form 29 June 2022; accepted 11 July 2022 (DOI: 10.30495/IJC.2022.1948621.1904)

ABSTRACT

In this study, we discuss the wet chemical synthesis and experimental analysis of zinc doped $Gd_2O_3(Gd_{2-x}Zn_xO_{3-\delta})$ nanoparticles where, $x=0, 0.1, 0.2, 0.3, 0.4,$ and 0.5 . The cubic crystalline structure is derived from XRD results and the existence of metal-oxide bond has been confirmed from FTIR studies. According to SEM and PSA analysis, the produced nanoparticles are found to be of nano size. The EDX data verified the presence of Gd, Zn, and O in the samples. Based on UV-visible spectroscopy, the band gap and λ_{max} values were computed. In an aqueous medium and under UV light irradiation, the photodegradation of Rhodamine B over Zn doped Gd_2O_3 nanoparticles was studied. It was observed that $Gd_{1.50}Zn_{0.50}O_{3-\delta}$ has exhibited 82% of photodegradation of the dye solution which further increased to 96% because of increasing the catalyst loading. The effect of pH and the concentration of the dye are also reported. According to the kinetic analysis, the photocatalysis process followed a pseudo-first-order kinetic model. A radical scavenger technique was used to further examine and identify the function of photoactive species.

Keywords: Co-precipitation method, Zn doped Gd_2O_3 catalysts, Photodegradation, Rhodamine B

1. Introduction

Chemical dyes which are mainly used in different industries and their effluents released into natural streams, are an environmental hazard. The water bodies are continuously being contaminated by the industrial effluent which contains organic pollutants such as dye stuffs from textiles, paint, paper, and plastic industries [1] which are genotoxic and also difficult to biodegrade. Various techniques are extensively used to eliminate dyes like synthetic dyes oxidation, coagulation, membrane separation, electrochemical process, surface-adsorption phenomena, biological process [2] and so on. Degradation procedures are discovered to be one of the advantageous processes that have been successfully

employed for dye removal from waste water under these chemical and physical methods [3]. Compared to bulk materials, metal oxide nanoparticles have special chemical and physical properties [4]. Methylene blue (MB) dye aqueous solution was subjected to the photocatalytic process with combined CdS-CuO nanoparticles (NPs) [5]. Utilizing semiconductor photocatalysts, a photo-induced oxidation method is used to destroy organic pollutants and render bacteria and viruses inactive when light is passed [6]. Scientists have developed several metal oxide semiconductor nanoparticles like Bi_2O_3 , TiO_2 , ZnO, and Fe_2O_3 which are found to have their application in photocatalysis due to their significant wide band gap, nontoxicity and high photosensitivity [7-9]. To explore their photocatalytic activity on the breakdown of organic dyes such as reactive yellow 145 (RY 145) and black 122 (DB 122) under a visible light source, it was reported that alumina

*Corresponding author:

E-mail address: samson@klu.ac.in (S. N. Arputharaj)

nanoparticles (both amorphous α - Al_2O_3 and gamma - Al_2O_3) were produced from tragacanth by sol-gel method. [10]. Due to its straight band gap and ability to excite holes and electrons when exposed to visible light, the CdS semiconductor is utilized as an effective photocatalyst in the breakdown of organic contaminants [11]. It is worth mentioning here that Eriochrome Black T, an azo dye was degraded 90% under visible light in 90 min by using CoCr_2O_4 cubic spinel nanoparticles which were synthesized via the green synthesis method [12]. In order to decolorize methyl green, the capability of a Fe (II)-orthophenanthroline photocatalyst doped on zeolite Na-Y was investigated [13]. TiO_2 nanoparticles have demonstrated a promising behavior as an effective photocatalytic material in a wide range of real applications, including the purification of water and air, the creation of energy, and self-cleaning surfaces. Metal oxide nanoparticles exhibit unique chemical and physical characteristics in comparison to bulk materials [14].

La^{3+} ions were added to the nanocrystalline Fe_3O_4 ferrite that Wang et al. synthesized to increase the adsorption capacity of magnetite for congo red [15]. According to Xu et al., doping with La^{3+} , Ce^{3+} , Er^{3+} , Gd^{3+} and Nd^{3+} was beneficial to NO_2^- adsorption [16]. By adding lanthanide ions to a TiO_2 matrix, it may be possible to concentrate an organic contaminant on the semiconductor's surface, proving titania's capacity as a photocatalyst [17]. Metronidazole was photodegraded using clinoptilolite nanoparticles (NC) assisted by SnS_2 - ZnS . (MZ). During the photoreduction of MZ over the SnZS-NC catalyst, the strength of the absorption peak around 234 nm grew while the peak at 321 nm sharply reduced, suggesting that the nitro group and nitrogen in metronidazole were decomposed and produced nitrite ion [18]. The synthesis, characterization, and photocatalytic degradation kinetics of the SnO_2 - BiVO_4 - CuO (SBC) catalyst have all been examined by Yousefi and Ejliah. The COD testing was conducted on photodegraded solutions, and the Hinshelwood plots revealed a slope of 0.01 min^{-1} , or a $t_{1/2}$ -value of 69.3 min [19]. Gadolinium nitrate hexahydrate ($\text{Gd}(\text{NO}_3)_3 \cdot 6\text{H}_2\text{O}$) and ethylamine were combined in a process to produce gadolinium oxide (Gd_2O_3) nanoparticles, according to Jeon et al. Gd_2O_3 nanoparticles were utilized as the photocatalyst when a number of azo dyes, such as methyl orange (MO), acid orange 7 (AO7), and acid yellow 23 (AY23), were exposed to UV light [20]. Dhanalakshmi et al. [21] successfully created gadolinium oxide (Gd_2O_3) nanorods utilizing a straightforward hydrothermal method for the photocatalytic degradation of chloramphenicol (CAP) medicine under UV light illumination. Under UV light

illumination, the Gd_2O_3 nanorods demonstrated increased efficacy compared to the conventional TiO_2 . The drug was quickly destroyed, according to the photocatalytic degradation results. The ideal conditions for efficient photocatalytic degradation were 50 mg of Gd_2O_3 nanorods and a drug concentration of 20 mg/mL. With seven electrons in 4f orbitals and an effective ionic radius of 0.0938 nm (Gd^{3+}), gadolinium (Gd) is recognized to be a useful element, while the effective ionic radius of Ti^{4+} is 0.0605 nm. So it has been claimed that Ti^{4+} can be replaced in part by Gd^{3+} [38-40]. The mechanism of Gd/TiO_2 and the formation of surface O_2 vacancy [22] have been reported. To enhance the photocatalytic capabilities of semiconductors TiO_2 and ZnO , the lanthanide oxide Gd_2O_3 has been added [23]. Due of its great chemical endurance, Gd_2O_3 is beneficial. Although its band gap energy varies depending on its structure [24, 25] from 3.8 eV to 5.4 eV, it absorbs UV light in the same region as Al_2O_3 . Photodegradation of 4-chlorophenol using $\text{Ag/Al}_2\text{O}_3$ - Gd_2O_3 photocatalyst [26] under UV light irradiation has been studied.

In this paper, we describe a successful attempt to synthesize parent Gd_2O_3 photocatalyst and Zn doped Gd_2O_3 nanoparticles using the chemical precipitation approach. By characterizing the synthesized particles, (Fig. 1), the photocatalytic behavior of the nanoparticles was investigated on the degradation of Rhodamine B (Rh B) dye, under UV light irradiation. The role of different parameters such as variation of dopant (Zn) concentration in Gd_2O_3 , the effect of photocatalyst loading and the influence of the pH of the dye on the photocatalyst was investigated as well.

2. Experimental

2.1. Materials

Gadolinium nitrate (99.9%, Thermo Fisher Scientific, India), zinc nitrate (96%, Merck, India), sodium hydroxide (97%, Merck, India), ethanol (99.9%, CS, China), and Rhodamine B (RhB) dye are the chemicals employed in this work (practical grade, Himedia, India). None of these materials were further purified before being employed. Double distilled water was used throughout the analysis. A light source of 11 W UV lamp is used for the photodegradation of the dye.

2.2. Facile chemical synthesis of Zn doped Gd_2O_3 nanoparticles

A straightway chemical precipitation method is used to produce parent Gd_2O_3 (undoped) and Zinc doped Gd_2O_3

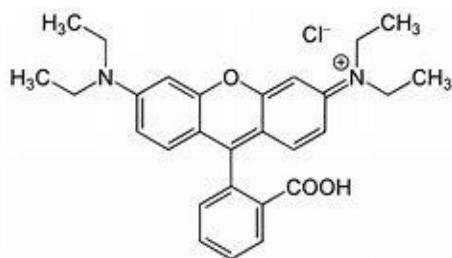
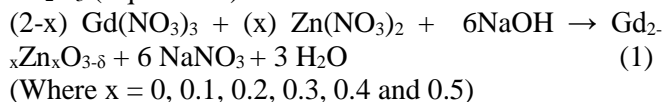


Fig. 1. The structure of Rhodamine B dye.

nanoparticles ($Gd_{2-x}Zn_xO_{3-\delta}$; where $x=0, 0.1, 0.2, 0.3, 0.4,$ and 0.5) [27]. In order to use this procedure, the following three solutions must be prepared separately by dissolving the necessary amounts of $Gd(NO_3)_3$, $Zn(NO_3)_2$, and $NaOH$ in double-distilled water at the necessary molar concentration. In this procedure, the produced $NaOH$ solution is continuously stirred on a magnetic stirrer at 950 rpm for approximately two hours at room temperature to the aqueous nitrate solutions taken in a beaker. The pH of the medium was maintained above 9 in order to get good precipitation [28]. Due to the production of hydroxides [$Gd(OH)_3+Zn(OH)_2$], the precipitation was immediate after the addition of the $NaOH$ solution. The precipitate is cleaned and purified using a 9:1 water and ethanol mixture after being vacuum-filtered. The precipitate mixture was then dried for a whole night at $60^\circ C$ before being further calcined in a muffle furnace for a total of three hours at each of the following increasing temperatures: 150, 300, 450, and $600^\circ C$ to produce phase-pure nanoparticles. **Table 1** lists the quantity of precursor salts utilized in the manufacture of Gd_2O_3 and Zn doped Gd_2O_3 nanoparticles. **Fig. 2** shows the flowchart for this response. Below is a list of the primary reactions involved in producing Gd_2O_3 and Zn-doped Gd_2O_3 (Equation 1).



2.3. Characterization

The powdered X-ray diffraction XRD studies of parent Gd_2O_3 and Zn doped Gd_2O_3 nanoparticles were conducted on the Shimadzu XRD6000 X-ray diffractometer using $Cu K\alpha$ ($k = 0.154059$ nm) radiation with a nickel filter at a voltage of 40 Kv at 30 mA current. The 2 scanning range was from 2° to 80° when using the continuous scan mode and a scan speed of $10^\circ \text{ min}^{-1}$. The unit cell parameter was measured using DOS programming. The infrared spectra of parent Gd_2O_3 and

Zn doped Gd_2O_3 nanoparticles were examined using the Fourier transform, a Shimadzu (IR Prestige 21) Spectrophotometer, and KBr pellet technique (4000 cm^{-1} to 400 cm^{-1}). The average particle size of parent Gd_2O_3 and Zn doped Gd_2O_3 nanoparticles for the PSA analysis was measured using a particle size analyzer (Zetasizer Ver.6.32 produced by Malvern Instruments Ltd.) at a measurement site of 4.65 mm. The surface morphology and elemental makeup of parent Gd_2O_3 and Zn doped Gd_2O_3 nanoparticles were examined using a SEM JEOL JSM-6610 running at 20 kV and outfitted with an energy dispersive X-ray (EDAX) spectrophotometer. The absorbance spectra of the nanoparticles were measured using a UV-Visible Spectrophotometer Shimadzu 1800. It has a diffused reflectance sphere with Teflon serving as the reference material. The diffused reflectance method was used to record spectra between the wavelength ranges of 200 nm and 600 nm from powder samples placed into a quartz cell. The Shimadzu LC2020 apparatus was used to obtain the HPLC and HPLC Mass chromatograms.

2.4. Photocatalytic experiments

By monitoring the breakdown of RhB dye in aqueous solution at room temperature, the photocatalytic activity of undoped Gd_2O_3 and Zn doped Gd_2O_3 nanoparticles was assessed. A pyrexphotoreactor, which comprises of a cylindrical pyrex glass reactor outfitted with an external UV light source with vertical irradiation, positioned on a magnetic stirrer at the bottom, was utilized to conduct the degradation process.

A set of typical photocatalytic reactions were performed using the synthesized parent and doped photocatalysts, individually, with 50 mL of aqueous RhB solution (0.0047g in 100 ml of 10^{-5} M) taken in the photoreactor. Each photocatalyst was added individually to the aforesaid dye solution (50 mL), and the suspension was first agitated in the dark for about 30 minutes to achieve the adsorption-desorption equilibrium of the dye before it was exposed to UV light. 2 mL of the solution (aliquots) was withdrawn after the predetermined amount of time, and the UV-visible spectra were recorded at 553 nm as shown [29]. Then the suspension was fed into the photoreactor and the UV light source (11 Watts) was turned on to record the photodegradation of each photocatalysts, as a function of time, at an interval of 20 minutes, for a period of one hour twenty minutes duration. All aliquots

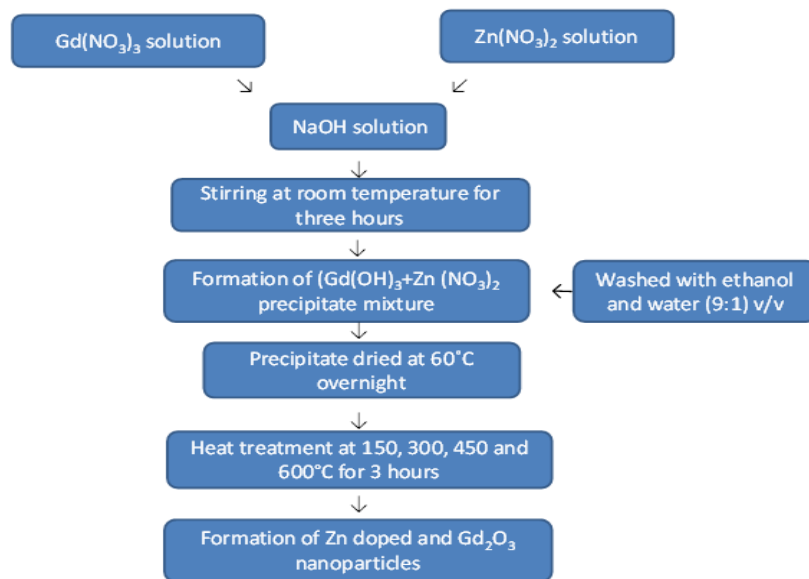


Fig. 2. Flow chart to prepare Zn doped Gd_2O_3 nanoparticles by chemical precipitation method.

Table 1. Amount of precursor salts used for the synthesis of Gd_2O_3 and Zn doped Gd_2O_3 nanoparticles [volume of each solution is 10 ml] by chemical precipitation method

Sample	Weight of $Gd(NO_3)_3$ (g)	Weight of $Zn(NO_3)_2$ (g)	Weight of NaOH (g)
Gd_2O_3	9.028	--	2.4
$Gd_{1.90}Zn_{0.10}O_{3-\delta}$	8.576	0.296	2.4
$Gd_{1.80}Zn_{0.20}O_{3-\delta}$	8.124	0.594	2.4
$Gd_{1.70}Zn_{0.30}O_{3-\delta}$	7.672	0.892	2.4
$Gd_{1.60}Zn_{0.40}O_{3-\delta}$	7.222	1.188	2.4
$Gd_{1.50}Zn_{0.50}O_{3-\delta}$	6.770	1.486	2.4

were taken and centrifuged to get rid of any potential photocatalysts at regular intervals. The maximum absorbance at 553 nm for each of the filtrates was then calculated. Equation 2 was used to calculate the dye [30] degradation percentage.

$$\text{Percentage of degradation} = \left(\frac{C_0 - C_t}{C_0} \right) \times 100 \quad (2)$$

Where, ' C_0 ' is the initial absorbance of the dye solution and ' C_t ' is the absorbance at time interval, respectively.

3. Results and Discussion

3.1. X-ray Diffraction studies

The XRD pattern of pure Gd_2O_3 and Zn doped Gd_2O_3 nanoparticles produced by chemical precipitation is illustrated in **Fig. 3**. Strong diffraction peaks can be seen in the XRD pattern, which shows that the synthesized nanoparticles are firmly crystalline. The XRD results were in good agreement with the data on Gd_2O_3 nanoparticles that had previously been reported [31]. The principle peaks obtained at 2θ value were 28.57, 47.52 and 56.43 corresponding to (222), (440) and (622) hkl values respectively. The other peaks obtained at 2θ values include 20.05, 33.12, 42.65, 57.78, 76.78, 78.40 and 79.40 corresponding to (211), (400), (134), (136),

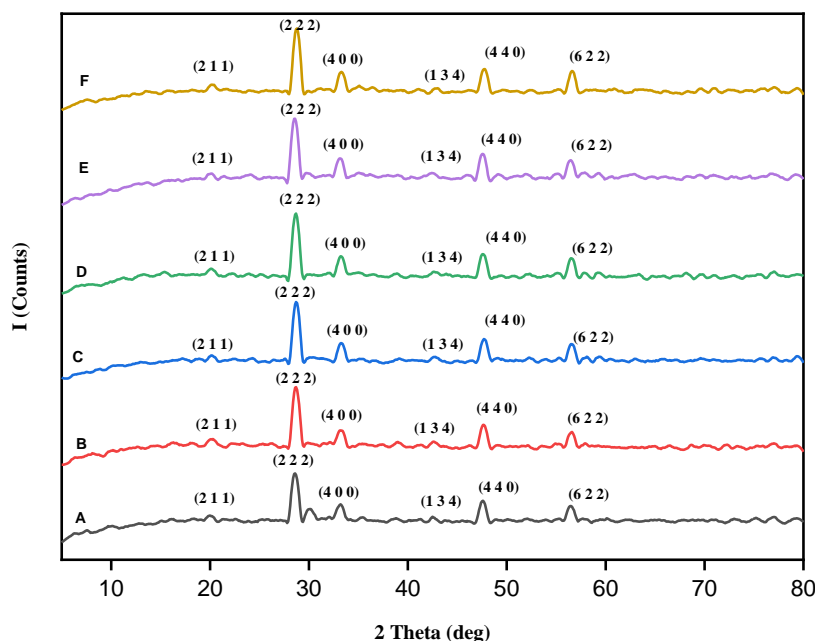


Fig. 3. XRD pattern obtained on Gd_2O_3 based nanoparticles A) Parent Gd_2O_3 , B) $Gd_{1.90}Zn_{0.10}O_{3-\delta}$, C) $Gd_{1.80}Zn_{0.20}O_{3-\delta}$, D) $Gd_{1.70}Zn_{0.30}O_{3-\delta}$, E) $Gd_{1.60}Zn_{0.40}O_{3-\delta}$, F) $Gd_{1.50}Zn_{0.50}O_{3-\delta}$.

(831), (662) and (048) planes respectively. The peak positions and their relative intensities obtained for the synthesized nanoparticles are well compared and indexed with the reported standard XRD data for Gd_2O_3 JCPDS card number 88-2165. From the diffraction pattern of Zn doped Gd_2O_3 samples, it is very clear that there is no trace of Zn related phases which confirms that the dopants (Zn) are well integrated into the Gd_2O_3 lattice [32]. Thus, there are no other (impurities) reflection peaks noticed in the diffraction pattern. This indicates that all the samples remain in single phase [33]. A slight change in XRD pattern is noted with different concentrations of zinc doping [34]. With an increase in doping concentration [35, 36], the strength of the diffraction peaks diminishes. The diffraction peaks are further indexed to a cubic crystalline structure with a lattice constant of $a = 10.82$ based on the XRD data [37, 38]. The materials are crystalline in nature, according to the strong peaks detected. Furthermore, there was no discernible impurity peak.

The average crystallite size was determined using all high intensity peaks seen in XRD patterns [39, 40]. Using the Debye-Scherrer formula, the crystallite size, D_x , was determined from the full width at half maximum (FWHM) of the XRD pattern. (Equation 3) [41],

$$D_x = \frac{k\lambda}{\beta \cos \theta} \quad (3)$$

Where β is the full width at half maximum (FWHM) of a diffraction peak, K is the shape factor approx. 0.91, λ is the wavelength of the X-ray source that equals 1.54 \AA and θ is the Bragg's angle. The calculated crystallite size values of Gd_2O_3 and Zn doped Gd_2O_3 are presented in **Table 2**. The average crystallite sizes calculated from the XRD data were 19.19 nm, 19.68 nm, 18.93 nm, 18.84 nm, 22.95 nm and 21.62 nm for undoped parent Gd_2O_3 , $Gd_{1.90}Zn_{0.10}O_{3-\delta}$, $Gd_{1.80}Zn_{0.20}O_{3-\delta}$, $Gd_{1.70}Zn_{0.30}O_{3-\delta}$, $Gd_{1.60}Zn_{0.40}O_{3-\delta}$ and $Gd_{1.50}Zn_{0.50}O_{3-\delta}$ respectively. The sample crystallite size ranged from 18 nm to 23 nm, which is consistent with the data stated as 8 to 20 nm [42].

Calculations were made to determine the strain brought on by crystal deformation and flaws in powders by using the formula [43]:

$$\varepsilon = \frac{\beta_{hkl}}{4 \tan \theta} \quad (4)$$

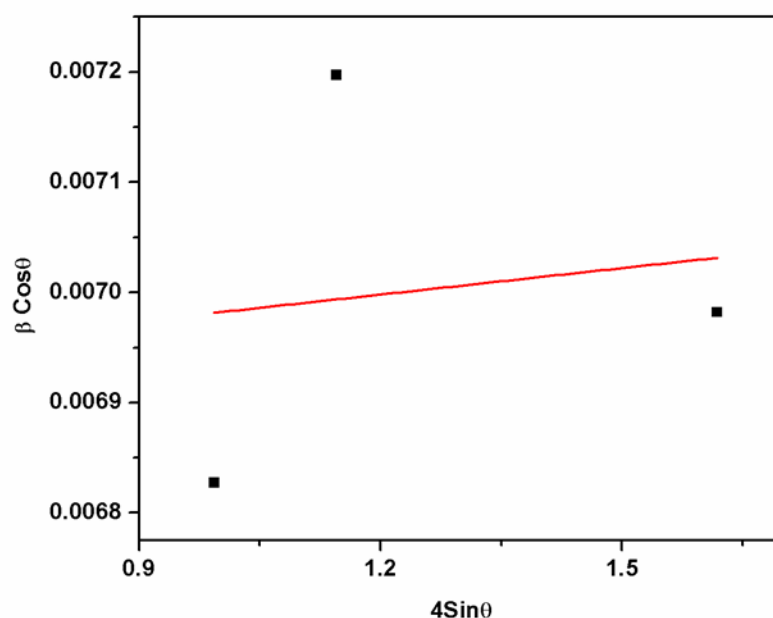
It was established from Equations 3 and 4, that the peak width caused by crystallite size changes as $1/\cos\theta$ strain changes as $\tan\theta$. The measured line breadth is simply the sum of Equations 3 and 4, assuming that the particle size and strain contributions to line broadening are independent to each other and both exhibit a Cauchy-like profile.

$$\beta_{hkl} = \frac{k\lambda}{D \cos \theta} + 4\varepsilon \tan \theta \quad (5)$$

From the above equation, we get

Table 2. Procedure for calculating the crystallite size for Gd_{1.50}Zn_{0.50}O_{3-δ} nanoparticles using W-H equations [43]

K	λ	2θ	B	4sinθ	βcosθ	Intercept (D)	C = Kλ/D
0.9	1.54	28.7341	0.3932	0.992531	0.006648013	0.00687	20.17467
		33.2437	0.4103	1.144215	0.00686185		
		47.6987	0.416	1.617333	0.006640602		

**Fig. 4.** W-H plot of Gd_{1.50}Zn_{0.50}O_{3-δ} nanoparticles.

$$\beta_{hkl\cos\theta} = \frac{K\lambda}{D} + 4\epsilon\tan\theta \quad (6)$$

W-H equations are those shown above. **Fig. 4** depicts a plot for as-prepared Gd_{1.50}Zn_{0.50}O_{3-δ} nanoparticles (best photocatalyst), with 4sinθ along the x-axis and β_{hkl}cosθ along the y-axis. The strain and crystallite size were calculated using the slope and y-intercept of the linear fit to the data, respectively. Equation 6 depicts the UDM, which takes into account the isotropic character of the crystal and the fact that material properties are independent of the direction along which they are measured. The strain was considered to be uniform in all crystallographic directions. The uniform deformation model for Gd_{1.50}Zn_{0.50}O_{3-δ} nanoparticles is shown in **Fig. 4**. The procedure for calculating the crystallite size for Gd_{1.50}Zn_{0.50}O_{3-δ} nanoparticles using W-H equations is presented in **Table 2**. The crystallite size calculated for Gd_{1.50}Zn_{0.50}O_{3-δ} nanoparticles by Debye-Scherrer formula and W-H model is almost the same. As per the literature, the crystalline characteristics of the samples were studied [44-46].

The theoretical density (D_p) was calculated by using the formula (Equation 7)

$$\text{Theoretical density, } D_{th} = z \frac{M}{N_A \times v} (\text{g.cm}^{-3}) \quad (7)$$

Where N_A is the Avogadro's number (6.023 x 10²³), Z is the number of chemical species in the unit cell, M is the sample molecular mass (g/mol), M is the molecular mass in gram per mole, V is the unit cell volume, and a³ is the lattice constant expressed in centimeters. The values were likewise consistent with the normal JCPDS data for Gd₂O₃ [88-2165], and the theoretical density of the Gd₂O₃ samples decreased with an increase in the dopant concentration of Zn. Using the Sauter formula, the samples' specific surface area (S) was calculated (Equation 8)

$$S = \frac{[6 \times (10)^3]}{D \times \rho} \quad (8)$$

Where "S" stands for the particular surface area, "D" for the crystallite size, and "ρ" for the density of the experimental materials employed. **Table 3** provides the

crystallographic characteristics acquired from nanoparticles of Gd_2O_3 and Zn doped Gd_2O_3 .

3.2. FTIR studies

The type of atomic bonds that are present in the molecule can be identified using FTIR spectroscopy. The FTIR spectroscopy was used to confirm that the

substance was an oxide after being heated in this manner. The FTIR spectra of Gd_2O_3 and Zn doped Gd_2O_3 nanoparticles with absorption peaks between 400 and 4000 cm^{-1} are shown in **Fig. 5**. The FTIR spectrum of Gd_2O_3 nanoparticles show significant absorption peaks at 441 cm^{-1} , 543 cm^{-1} , 1382 cm^{-1} , 1639 cm^{-1} and

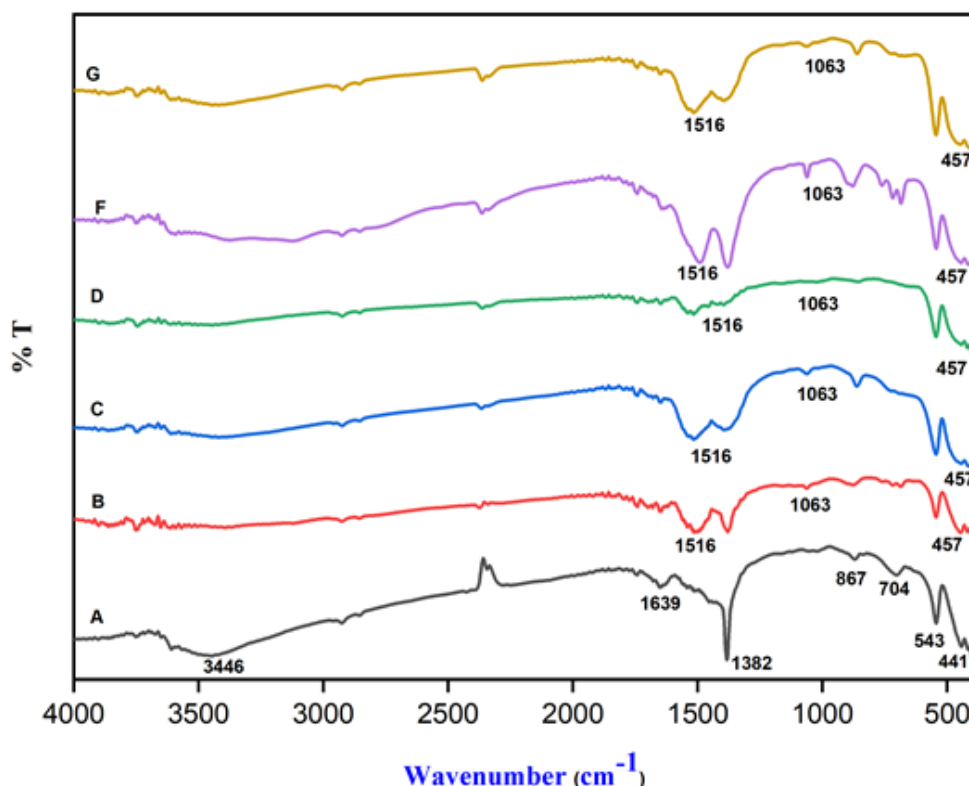


Fig. 5. FTIR spectra obtained on Gd_2O_3 based nanoparticles A) Parent Gd_2O_3 , B) $Gd_{1.90}Zn_{0.10}O_{3-\delta}$, C) $Gd_{1.80}Zn_{0.20}O_{3-\delta}$, D) $Gd_{1.70}Zn_{0.30}O_{3-\delta}$, E) $Gd_{1.60}Zn_{0.40}O_{3-\delta}$, F) $Gd_{1.50}Zn_{0.50}O_{3-\delta}$.

Table 3. Crystallographic parameters obtained on Gd_2O_3 and Zn doped Gd_2O_3 nanoparticles.

Sample	Crystal structure	Unit cell parameter (\AA)	Unit cell volume (\AA^3)	Crystallite size (Debye-Scherrer formula) (nm)	Theoretical density (gcm^{-3})	Specific Surface area (m^2/g)
Gd_2O_3 (JCPDS No. 882165)	Cubic (B.C.)	10.79	1256.22	--	7.66	--
Parent Gd_2O_3	Cubic (B.C.)	10.82	1267.15	19.19	7.59	215.6
$Gd_{1.90}Zn_{0.10}O_{3-\delta}$	Cubic (B.C.)	10.81	1265.64	19.68	7.41	365.1
$Gd_{1.80}Zn_{0.20}O_{3-\delta}$	Cubic (B.C.)	10.79	1259.67	18.93	7.25	351.0
$Gd_{1.70}Zn_{0.30}O_{3-\delta}$	Cubic (B.C.)	10.81	1266.62	18.84	7.02	339.1
$Gd_{1.60}Zn_{0.40}O_{3-\delta}$	Cubic (B.C.)	10.82	1266.84	22.95	6.83	233.4
$Gd_{1.50}Zn_{0.50}O_{3-\delta}$	Cubic (B.C.)	10.81	1263.76	21.62	6.65	373.0

3446 Gd_2O_3 . A strong intense absorption peak at 543 cm^{-1} is the characteristic peak of Gd_2O_3 [47]. According to published data [48], the bands at 543 cm^{-1} and 441 cm^{-1} correspond to the Gd-O vibration of Gd_2O_3 . The vibrations of O-H stretching and deformation, accordingly, are what caused the bands to arise at 3446 cm^{-1} and 1639 cm^{-1} , respectively [49]. The usual metal-oxide vibration band is displayed between 1000 and 400 cm^{-1} [50]. Additionally, it has been noted in the literature that CO_3^{2-} anion groups are responsible for the absorption bands in the $1300\text{--}1600\text{ cm}^{-1}$ range and for the absorption peak at 3410 cm^{-1} due to H_2O , which nanocrystalline materials typically absorb from the environment due to their high surface-to-volume ratios [51]. In general, the FTIR absorption peaks of solids are associated with the vibration of ions in the crystal lattice [52]. The stretching and bending vibrations of O-H and C=O, respectively, are represented by the particular peaks that emerged at 3446 cm^{-1} and 1639 cm^{-1} , respectively [33]. The presence of water molecules (O-H), which the samples have absorbed, is what causes these stretching and bending vibrational modes [53-55]. These findings demonstrate the hygroscopic character of the produced nanoparticles [56, 57]. Along with the absorption peaks at 1063 cm^{-1} and 1602 cm^{-1} , which are the distinctive absorption peaks of Zn dopant, the new peak at 457 cm^{-1} indicates the presence of the Zn-O bond [58-63].

3.3. Particle size analysis

The particle size distribution curves of Gd_2O_3 and Zn doped Gd_2O_3 nanoparticles are shown in **Fig. 6**. The samples were exposed to a particle size analyzer after being sonicated in distilled water for roughly 20 minutes

for all measurements. **Table 4** displays statistics on particle properties. The samples were visible between 50.0 and 491.0 nm. The higher particle size may be the result of grains clumping together during the calcination process. [64]. Further, double peaks observed in the analysis might be due to the particles that are not dispersed [65].

3.4. EDX analysis

From EDX spectral analysis, as shown in **Fig. 7**, the elemental composition of the parent Gd_2O_3 and Zn doped Gd_2O_3 nanoparticles was determined. The spectra display the gadolinium, oxygen, and zinc peak locations. For the doped materials generated at various molar ratios, the analysis has confirmed the existence of the dopant Zn with increasing weight % in diverse compositions. The quantitative EDX data show that, within the experimental range, the percentage weights (at percent) of the components are similar to their nominal composition. Conditions throughout the experiment could account for a slight difference in the dopant level in the finished product. The composition of the synthesized nanoparticles for the parent and dopant are given in **Table 5**. The EDX results confirmed that the prepared pure and Zn doped Gd_2O_3 nanoparticles are free of impurities.

3.5. SEM studies

SEM is used to examine the topographical pictures of the freshly manufactured particles. **Fig. 8** displays SEM images of Gd_2O_3 nanoparticles with Zn doping and without Zn doping. The SEM photographs revealed the presence of well-defined circular grains of the samples. The size of the grains was found to be in between 100–400 nm which is in accordance with particle size

Table 4. Particle characteristics data obtained on Gd_2O_3 and Zn doped Gd_2O_3 nanoparticles

Sample	Peak 1		Average
	Intensity (%)	Width (d. nm)	Particle Size (nm)
Parent Gd_2O_3	100	61.71	345.3
$\text{Gd}_{1.90}\text{Zn}_{0.10}\text{O}_{3-\delta}$	100	27.28	142.6
$\text{Gd}_{1.80}\text{Zn}_{0.20}\text{O}_{3-\delta}$	100	64.75	201.2
$\text{Gd}_{1.70}\text{Zn}_{0.30}\text{O}_{3-\delta}$	100	49.50	50.28
$\text{Gd}_{1.60}\text{Zn}_{0.40}\text{O}_{3-\delta}$	100	223.3	355.5
$\text{Gd}_{1.50}\text{Zn}_{0.50}\text{O}_{3-\delta}$	100	191.3	491

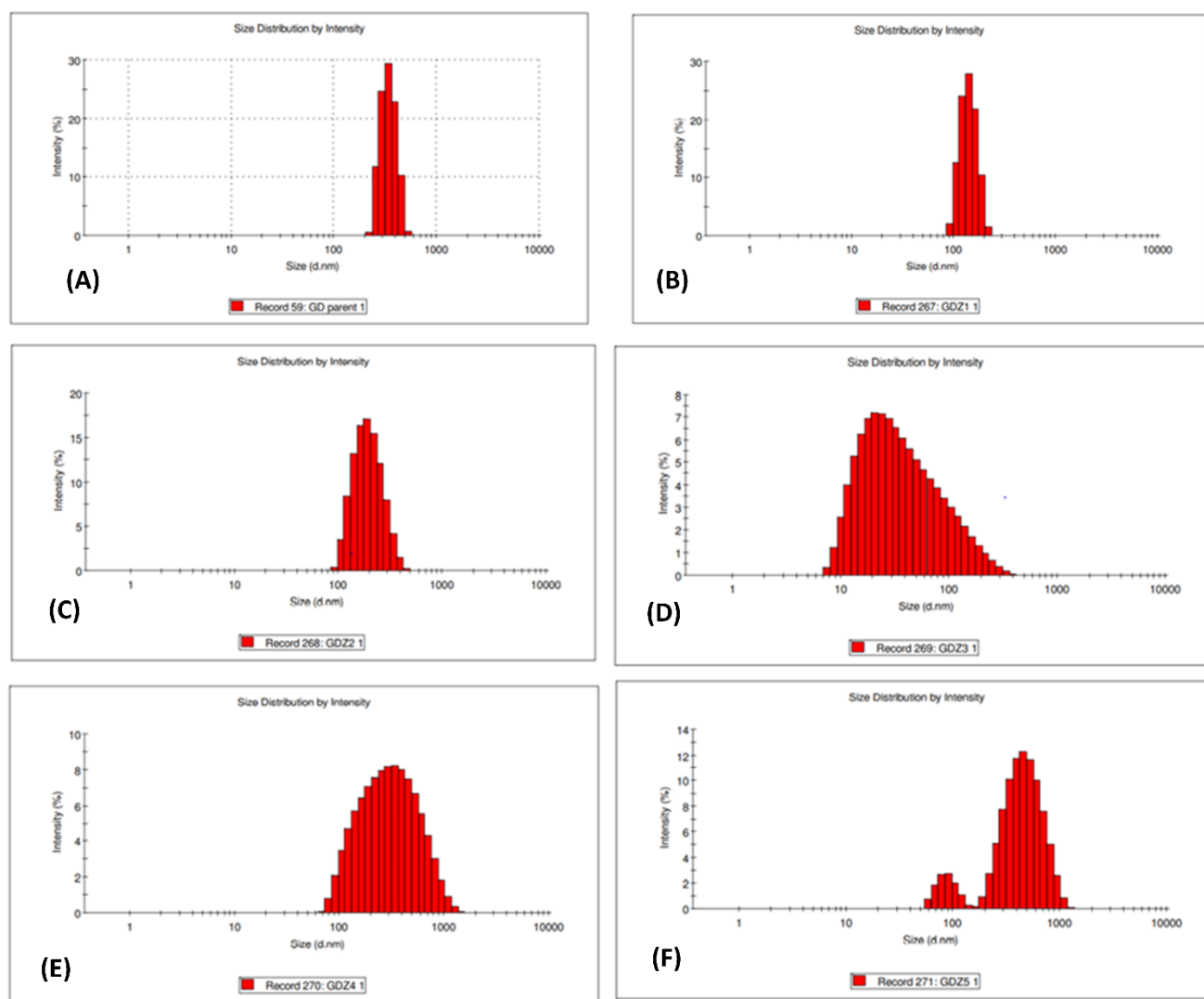


Fig. 6. Particle size distribution curves obtained on Gd_2O_3 based nanoparticles A) Parent Gd_2O_3 , B) $Gd_{1.90}Zn_{0.10}O_{3-\delta}$, C) $Gd_{1.80}Zn_{0.20}O_{3-\delta}$, D) $Gd_{1.70}Zn_{0.30}O_{3-\delta}$, E) $Gd_{1.60}Zn_{0.40}O_{3-\delta}$, F) $Gd_{1.50}Zn_{0.50}O_{3-\delta}$.

distribution data. The aggregation of smaller grains during the high-temperature calcination of samples may be the cause of the existence of bigger grains.

3.6. Studies on optical properties

Using a UV-visible method, the optical properties of Gd_2O_3 and Zn doped Gd_2O_3 nanoparticles were investigated. **Fig. 9** displays the UV-visible absorption spectra of pure and Zn-doped Gd_2O_3 nanoparticles, which were discovered in the 200 nm–800 nm wavelength range. Gd_2O_3 and Zn doped Gd_2O_3 nanoparticles have a large peak between 304 and 310 nm, as can be seen in the graph. The produced Gd_2O_3 nanoparticles UV spectra have a low intensity peak at 304 nm. [66]. Importantly, the UV spectrum of calcined sample at 600 °C indicates two absorption peaks at 280 nm (sharp) and 304 nm (broad) in Gd_2O_3 nanoparticles. The valence band electrons of the photocatalyst move

into the conduction band when exposed to UV light. Continuous creation of holes in the valence band and electrons in the conduction band come from this transition. Additionally, Zn doping produces an emission that is visible at about 380 nm. By using a reflectance method and the Tauc hypothesis, the band gap energy was discovered [67–69]. Equation 9 is the Tauc [70] plot to determine the direct band gap for Gd_2O_3 and Zn doped Gd_2O_3 nanoparticles.

$$ah\nu = A(h\nu - E_g)^{1/2} \quad (9)$$

where ‘ α ’ is the absorption coefficient, ‘ A ’ is a constant and $n = 1/2$ for direct band gap semiconductor. An extrapolation of the linear region of a plot of $(\alpha h\nu)^2$ vs $h\nu$ gives the value of the optical band gap (E_g) as shown in **Fig. 10**. The band gap of parent Gd_2O_3 was found to be 4.76 eV which is very close to reported value of 5.4 eV [71]. In general, the band gap values incalced samples

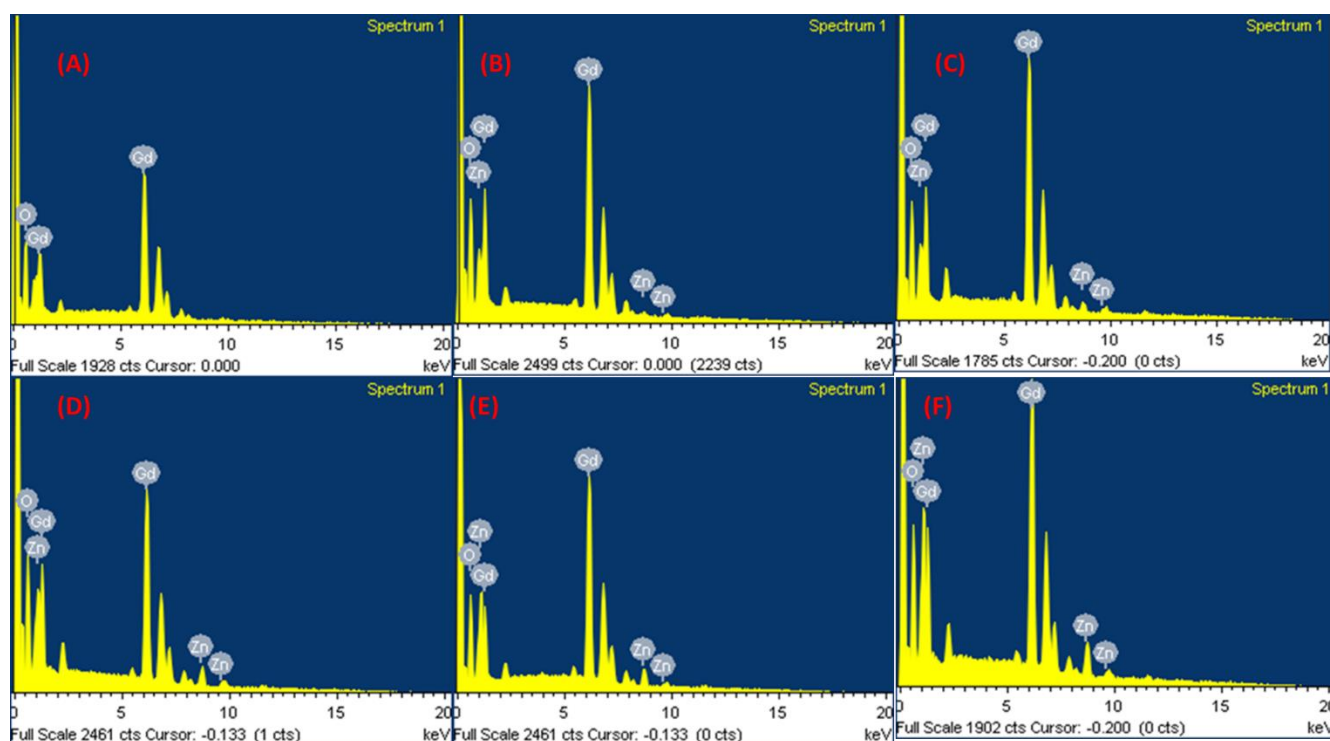


Fig. 7. EDX spectra obtained on Gd_2O_3 based nanoparticles A) Parent Gd_2O_3 , B) $Gd_{1.90}Zn_{0.10}O_{3-\delta}$, C) $Gd_{1.80}Zn_{0.20}O_{3-\delta}$, D) $Gd_{1.70}Zn_{0.30}O_{3-\delta}$, E) $Gd_{1.60}Zn_{0.40}O_{3-\delta}$, F) $Gd_{1.50}Zn_{0.50}O_{3-\delta}$.

Table 5. Elemental composition data obtained on Gd_2O_3 and Zn doped Gd_2O_3 nanoparticles.

Sample	Atomic weight % of the elements		
	Gd	Zn	O
Parent Gd_2O_3	28.09	0	71.91
$Gd_{1.90}Zn_{0.10}O_{3-\delta}$	28.66	0.97	70.37
$Gd_{1.80}Zn_{0.20}O_{3-\delta}$	31.38	3.08	65.54
$Gd_{1.70}Zn_{0.30}O_{3-\delta}$	23.26	5.14	71.59
$Gd_{1.60}Zn_{0.40}O_{3-\delta}$	30.70	6.38	62.92
$Gd_{1.50}Zn_{0.50}O_{3-\delta}$	27.20	7.95	64.84

ranges from 5.0 – 5.6 eV were well matched with the literature [71]. The literature states that changes in band gap values can be linked to the degree of structural order-disorder present in the lattice, which affects the distribution of energy levels inside the band gap. The experimental parameters used, such as heat treatment, temperature, and even processing time, as well as the synthesis techniques used has an impact on the E_g values. These variables can encourage or prevent the development of structural flaws, which in turn affect the degree of structural order-disorder in the materials and, as a result, the number of intermediary energy levels in the band gap [51]. Further, the band gap values for Zn doped Gd_2O_3 with varying concentration were found to

be 4.41 eV ($Gd_{1.90}Zn_{0.10}O_{3-\delta}$), 4.23 eV ($Gd_{1.80}Zn_{0.20}O_{3-\delta}$), 3.92 eV ($Gd_{1.70}Zn_{0.30}O_{3-\delta}$), 2.71 eV ($Gd_{1.60}Zn_{0.40}O_{3-\delta}$) and 3.70 eV ($Gd_{1.50}Zn_{0.50}O_{3-\delta}$) which are in line with reported value for parent oxide [71].

3.7. Photocatalytic studies

3.7.1. Photocatalytic activity

The photocatalytic degradation of the pollutant, Rhodamine B (RhB) dye, was carried out in a photoreactor and the reaction parameters were altered to enhance the process of photodegradation efficiency. The photocatalysis process involves the photodegradation of aqueous solution of RhB dye using pure Gd_2O_3 and Zn doped Gd_2O_3 nanoparticles. It was observed that there

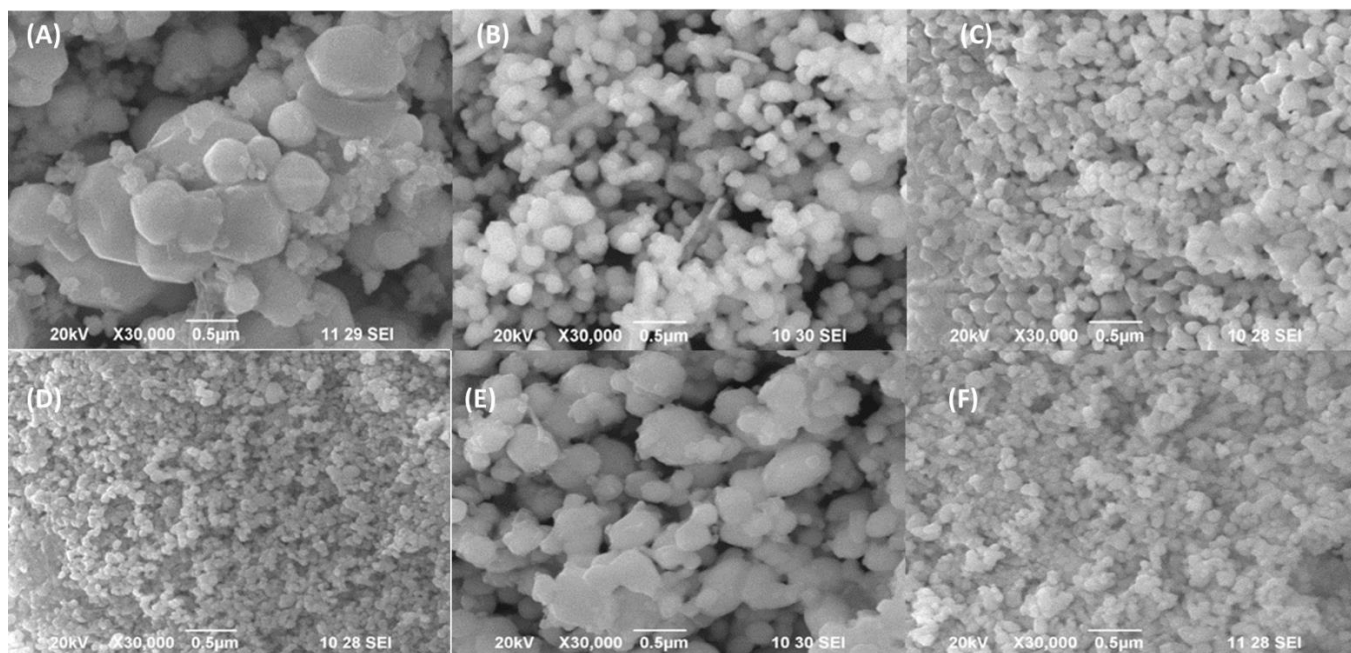


Fig. 8. SEM photographs obtained on Gd_2O_3 based nanoparticles A) Parent Gd_2O_3 , B) $Gd_{1.90}Zn_{0.10}O_{3-\delta}$, C) $Gd_{1.80}Zn_{0.20}O_{3-\delta}$, D) $Gd_{1.70}Zn_{0.30}O_{3-\delta}$, E) $Gd_{1.60}Zn_{0.40}O_{3-\delta}$, F) $Gd_{1.50}Zn_{0.50}O_{3-\delta}$.

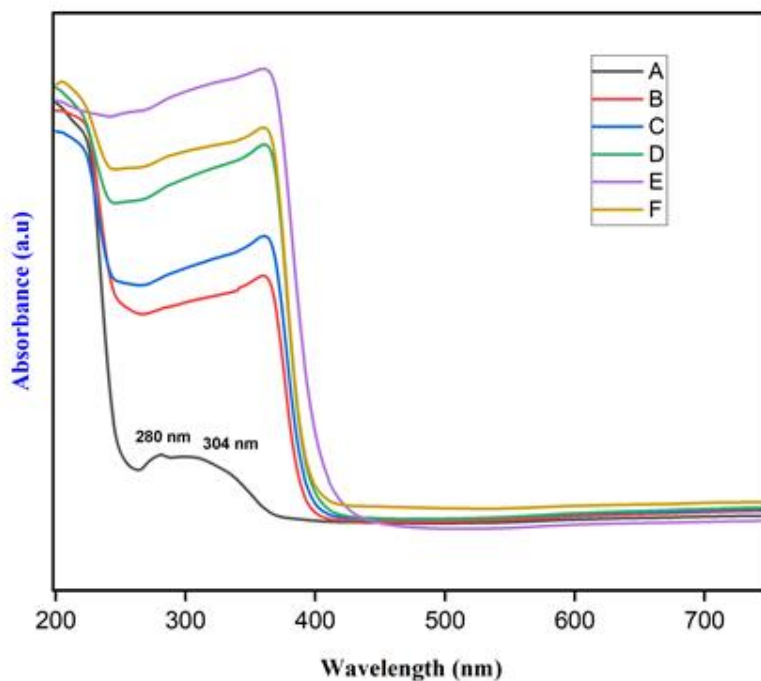


Fig. 9. UV visible spectra obtained on Gd_2O_3 based nanoparticles A) Parent Gd_2O_3 , B) $Gd_{1.90}Zn_{0.10}O_{3-\delta}$, C) $Gd_{1.80}Zn_{0.20}O_{3-\delta}$, D) $Gd_{1.70}Zn_{0.30}O_{3-\delta}$, E) $Gd_{1.60}Zn_{0.40}O_{3-\delta}$, F) $Gd_{1.50}Zn_{0.50}O_{3-\delta}$.

wasn't any degradation when the dye is mixed with water in the mixed state to form an aqueous dye solution and stirred at dark. But a significant degradation of the dye was noted in the presence of the as-synthesized photocatalyst nanoparticles under UV light irradiation and the percentage degradation has also been enhanced effectively in the presence of doped photocatalyst.

The photocatalytic degradation performance of pure and doped Gd_2O_3 nanoparticles samples (as photocatalyst) was studied using RhB dye (as pollutant) under UV light source [Figs. 11 and 13]. The degradation percentage of the dye was recorded by using a pre fixed amount of as-synthesized Gd_2O_3 and zinc doped Gd_2O_3 photocatalysts, with different concentrations as $Gd_{2-x}Zn_xO_{3-\delta}$ (where $x = 0, 0.1, 0.2, 0.3, 0.4$ and 0.5), illuminated with UV light

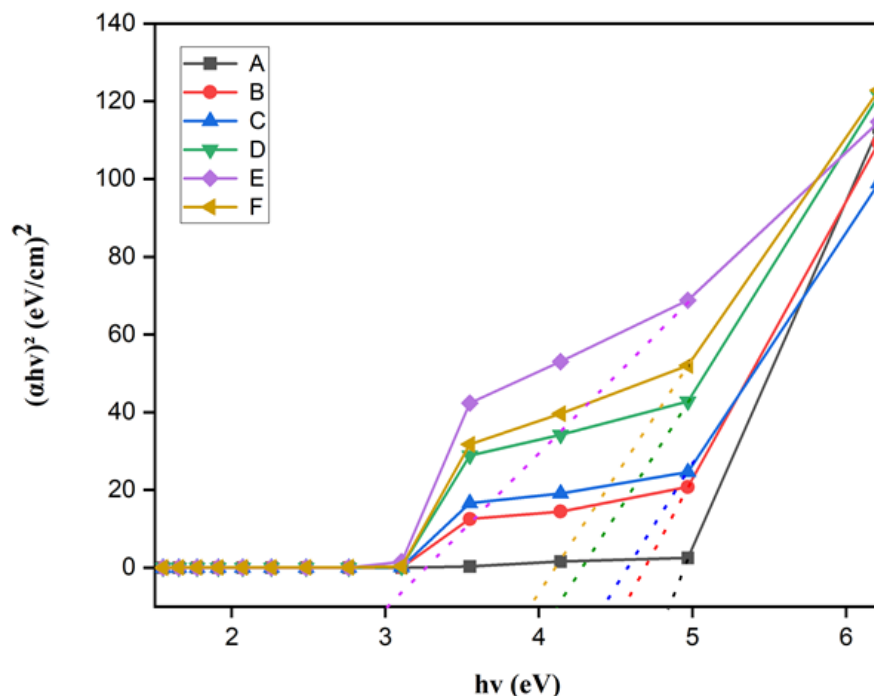


Fig. 10. Band gap plot obtained on Gd₂O₃ based nanoparticles A) Parent Gd₂O₃, B) Gd_{1.90}Zn_{0.10}O_{3-δ}, C) Gd_{1.80}Zn_{0.20}O_{3-δ}, D) Gd_{1.70}Zn_{0.30}O_{3-δ}, E) Gd_{1.60}Zn_{0.40}O_{3-δ}, F) Gd_{1.50}Zn_{0.50}O_{3-δ}.

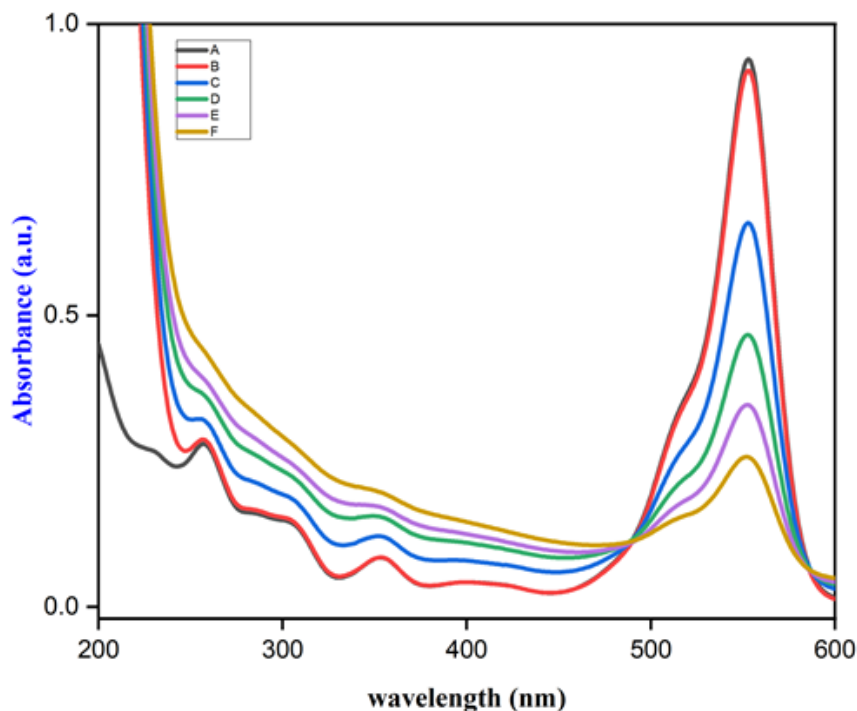


Fig. 11. Photo-degradation spectra obtained on pure Gd₂O₃ nanoparticles (A) At initial stage, (B) After 0 minutes, (C) After 20 minutes, (D) After 40 minutes, (E) After 60 minutes and (F) After 80 minutes.

recorded at various time intervals as 0, 20, 40, 60 and 80 minutes. On photo irradiation of RhB dye in presence of catalysts, the intensity of the absorption band was observed at $\lambda_{\text{max}} = 552$ nm, which uniformly decreased with increased irradiation time thereby indicating the

degradation of RhB by the synthesized nanoparticles. The degradation rate of RhB dye in presence of Gd₂O₃ nanoparticles with time T is shown in **Fig. 11**.

The adsorption capacity of the dye on the metal oxide plays a vital parameter for the surface reaction. This

includes the various parameters such as surface density, pore size distribution and morphology of the particle surface. Surface adsorption is a time dependent process. The amount of photocatalyst adsorbed increased progressively with time and temperature as well [72]. The rate of degrading capability of pure and undoped Gd_2O_3 nanoparticles shows a slow and gradual degradation of the dye as shown in **Fig. 11**, which may be attributed to the photosensitization of the dye [73]; the maximum percentage degradation using pure Gd_2O_3 nanoparticles was observed to be 72 % at 80 minutes of irradiation time. The presence of gadolinium, which has half-filled orbitals that operate as a center of attraction for charge carriers to speed up interfacial charge transfer processes, is what causes the accelerated photocatalytic degradation [74]. Additionally, superoxide and hydroxyl radicals, which are extremely reactive and oxidative in water, might oxidise the pigment as an organic pollution. The capacity of pure Gd_2O_3 nanoparticles to degrade azo dyes like methyl orange (MO), acid orange 7 (AO7), and acid yellow 23 can also be compared to their photocatalytic activity (AY23). According to the literature [75], MO and AO7 showed a degradation of about 79 % and AY23 showed 59 % degradation in presence Gd_2O_3 nanoparticles under UV light irradiation.

However, percentage degradation of the dye was improved when Gd_2O_3 nanoparticles were doped with zinc ions at varying molar concentration ratios as $Gd_{1.90}Zn_{0.10}O_{3-\delta}$, $Gd_{1.80}Zn_{0.20}O_{3-\delta}$, $Gd_{1.70}Zn_{0.30}O_{3-\delta}$, $Gd_{1.60}Zn_{0.40}O_{3-\delta}$ and $Gd_{1.50}Zn_{0.50}O_{3-\delta}$ (**Fig. 12**). It was observed that under the same photocatalytic conditions, Zn doped Gd_2O_3 photocatalysts show greater photodegradation than that of pure and undoped Gd_2O_3 samples at 80 minutes irradiation time. This is mainly due to the presence of doping [76-78]. The inclusion of Zn ions in the lattice of Gd_2O_3 nanoparticles, which reduces electron-hole pair recombination and increases the number of free electrons and holes available for the generation of free radical ions, is thought to be the cause of the higher degradation rate. In the absence of a light source (dark), the degradation % of RhB was found to be less than 12%. On UV irradiation, the photodegradation of Rh B with pure Gd_2O_3 nanoparticles was recorded as 72% after 80 minutes irradiation, which has eventually shown greater percentage of degradation with Zn doping. As the concentration of Zn dopant increased, percentage degradation also increased [79] and the maximum photo conversion of RhB by $Gd_{1.50}Zn_{0.50}O_{3-\delta}$ after 80 minutes, was noted as 82% (**Fig. 12**). The higher photocatalytic activity of $Gd_{1.50}Zn_{0.50}O_{3-\delta}$ is due to the increased catalyst concentration [80]. Further, it is also observed

that the activity of $Gd_{1.60}Zn_{0.40}O_{3-\delta}$ is less, in spite of its lower band gap of 3.01eV. This might be due to inefficient transfer of photogenerated electrical charges on to the surface, which were later lost due to recombination [81].

The reaction follows pseudo first order and the kinetics was evaluated using the formula (Equation 10) and plotted as shown in **Fig. 13**.

$$\ln \frac{C_t}{C_0} = -kt \quad (10)$$

Where C_0 is the initial concentration of the dye, C is the concentration at time t, k is the rate constant of the first-order reaction.

Further, the degradation rate constant (k) has shown a gradual rise from pure Gd_2O_3 nanoparticles to Zn doped photocatalysts with varying molar concentrations. Thus, from the above results, it is evident that the incorporation of Zn dopant can synergistically enhance the photodegradation of pure Gd_2O_3 nanoparticles (**Fig. 13**). Moreover, the apparent rate constant 'k' values of $Gd_{1.90}Zn_{0.10}O_{3-\delta}$, $Gd_{1.80}Zn_{0.20}O_{3-\delta}$, $Gd_{1.70}Zn_{0.30}O_{3-\delta}$, $Gd_{1.60}Zn_{0.40}O_{3-\delta}$ and $Gd_{1.50}Zn_{0.50}O_{3-\delta}$ have been calculated as 0.022, 0.026, 0.024, 0.028, 0.018 and 0.028 respectively. It was noted that $Gd_{1.60}Zn_{0.40}O_{3-\delta}$ shows less rate constant compared to other samples. Further, the degradation rate constant (k) has shown a gradual rise from pure Gd_2O_3 nanoparticles to Zn doped photocatalysts with varying molar concentrations. The findings showed that the catalytic activity of parent Gd_2O_3 photocatalysts is significantly lower than that of all other compositions of pure Zn doped Gd_2O_3 photocatalysts. Many kinetics models make the assumption that the rate of a reaction is dependent on the number of electrons in the conduction band (or valence band holes). This strategy, nevertheless, can occasionally be incorrect since the electrons and the substrate molecules are present in separate phases and cannot easily interact with one another [82]. Additionally, in thermal heterogeneous catalysis, the magnitude of the rate constant and the strength of the adsorption typically depend on the structure of the reactant [83]. These negative results can sometimes be correlated to the Overall Volumetric Rate of Photon Absorption (OVRPA) [84] which involves catalyst concentration optimization [85,86]. From the above results, $Gd_{1.50}Zn_{0.50}O_{3-\delta}$ was found to be the optimum photocatalyst sample that has shown high degradation efficiency. The photodegradation pathway can be illustrated as per the literature [87-92]. **Fig. 14** illustrates the mechanism for the UV photocatalytic degradation of RhB in the presence of Zn doped Gd_2O_3 based on the literature mentioned above. The kinetic

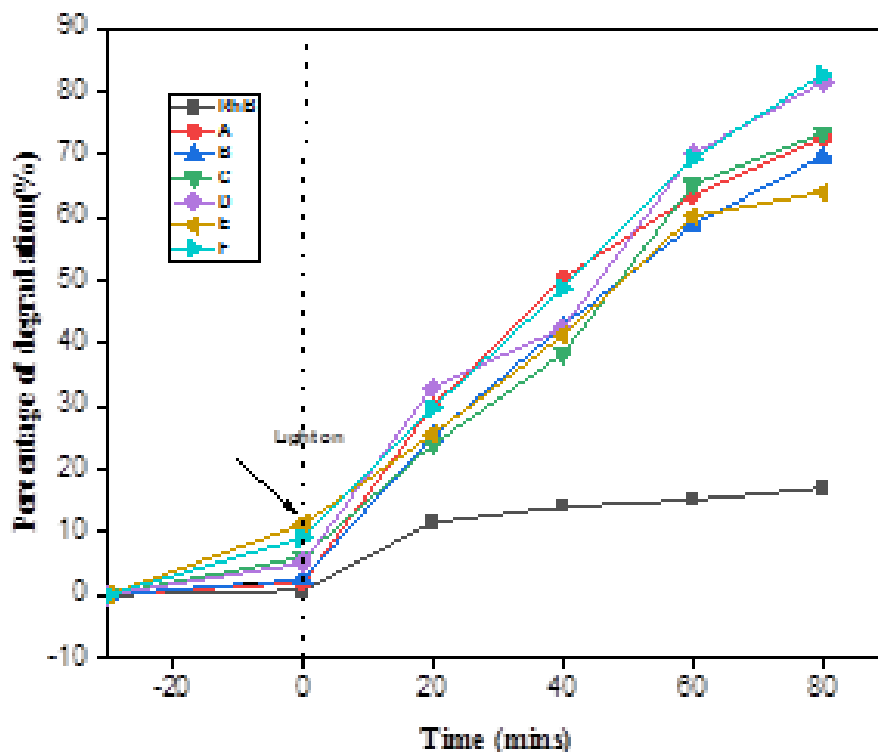


Fig. 12. Photodegradation spectra of RhB using the photocatalysts A) Parent Gd_2O_3 , B) $Gd_{1.90}Zn_{0.10}O_{3-\delta}$, C) $Gd_{1.80}Zn_{0.20}O_{3-\delta}$, D) $Gd_{1.70}Zn_{0.30}O_{3-\delta}$, E) $Gd_{1.60}Zn_{0.40}O_{3-\delta}$, F) $Gd_{1.50}Zn_{0.50}O_{3-\delta}$.

aspect of photo degradation has been discussed elaborately in the literature [93-95]. Thus, different parameters were analyzed using the above catalyst. The study investigates the following essential parameters: (i) influence of photocatalyst loading and (ii) influence of pH of the dye on the photocatalyst.

3.7.2. Influence of photocatalyst loading

The influence of photocatalyst loading on the photodegradation of Rh B was investigated with the doped photocatalyst, $Gd_{1.50}Zn_{0.50}O_{3-\delta}$, which resulted in the highest degradation efficiency. The study was investigated by altering the photocatalyst loading (amount) as 0.025 g. L^{-1} , 0.05 g. L^{-1} , 0.075 g. L^{-1} and 0.1 g. L^{-1} . For 80 minutes, the effectiveness of the aforesaid catalyst's photocatalytic activity was demonstrated. It was observed that as the photocatalyst loading dosage increases, the degradation efficiency has increased as well. When the loading of the photocatalyst was increased, the availability of the number of active sites on the surface area of the sample increases, which subsequently resulted in the creation of larger number of superoxide and hydroxyl radicals [96-98]. Moreover, when the catalyst loading increases, the quantity of photons that get adsorbed also increases resulting in the increased rate of degradation [79]. The enhancement of

photocatalytic activity of NiO based nanoparticles was already reported in the literature. According to reports, the amount of NiO injected has a considerable impact on the process efficiency [99]. The percentage degradation of Rh B by using different loading of $Gd_{1.50}Zn_{0.50}O_{3-\delta}$ was recorded as 72.58%, 82.82%, 94.02% and 96.18% (**Fig. 15**) for a dosage of 0.025g, 0.05g, 0.075g and 0.1g of the photocatalyst respectively. Thus, the highest degradation of 96% was observed for the highest dosage (0.1 g) of the photocatalyst, which clearly proved the influence of increased catalyst loading on the efficiency of greater degradation.

3.7.3. Influence of pH of the dye on photocatalyst

The influence of pH, alters the charge and the number of active adsorption sites on the photocatalysts as well as on the pollutants [100]. Photocatalytic experiments were carried out at different pH values ranging from 2.5, 4.3, 7, 10 and 11, for a fixed dye concentration using 0.1g of $Gd_{1.50}Zn_{0.50}O_{3-\delta}$ shown in **Fig. 16**. It was noted that percentage degradation is comparatively less at lower pH of 2.5 which increases with acidity, reaching 96 % at a pH of 4.3 i.e., the rate of degradation is less (50%) at lower acidic pH (2.5), which increases at higher acidic pH (4.3) reaching a percentage degradation of 96%.

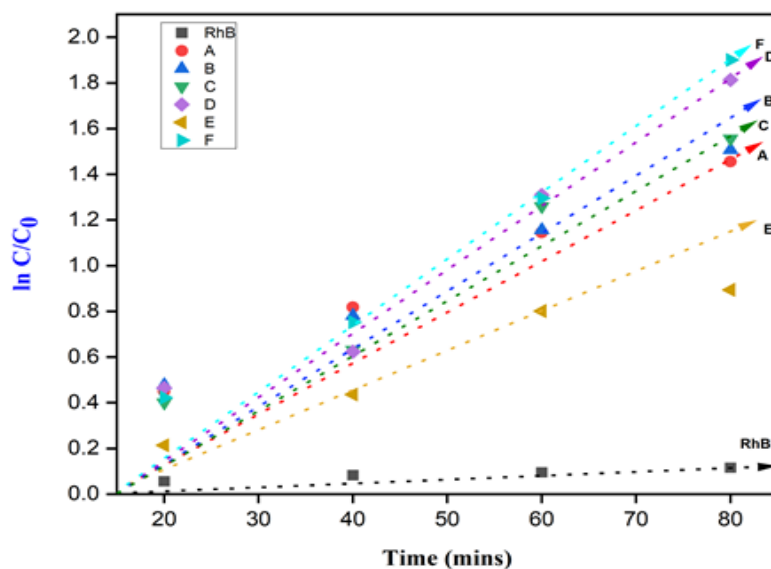


Fig. 13. First order kinetics plot of RhB using the photocatalysts A) Parent Gd_2O_3 , B) $Gd_{1.90}Zn_{0.10}O_{3-\delta}$, C) $Gd_{1.80}Zn_{0.20}O_{3-\delta}$, D) $Gd_{1.70}Zn_{0.30}O_{3-\delta}$, E) $Gd_{1.60}Zn_{0.40}O_{3-\delta}$, F) $Gd_{1.50}Zn_{0.50}O_{3-\delta}$.

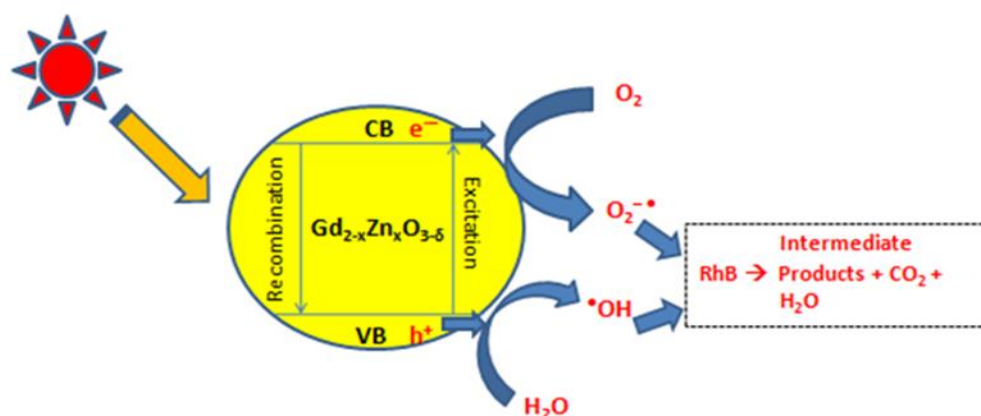


Fig. 14. Proposed mechanism for the UV photocatalytic degradation of RhB in presence of Zn doped Gd_2O_3 .

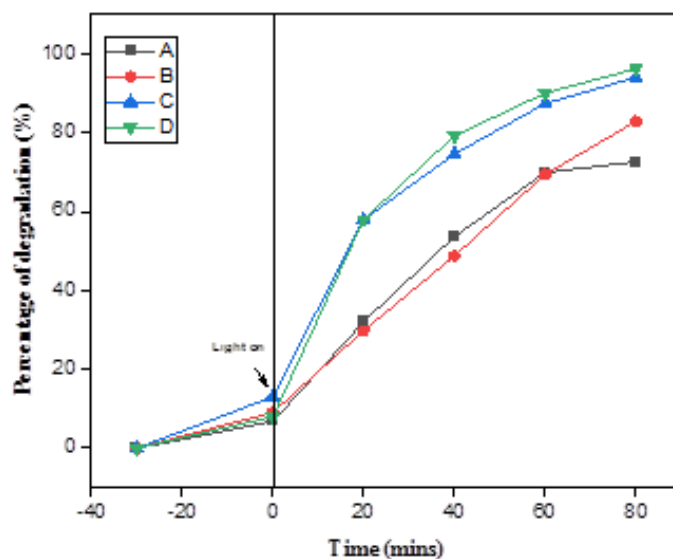


Fig. 15. Degradation spectra of photocatalysts loaded with A) 0.025g, B) 0.05g, C) 0.075g, D) 0.1g of $Gd_{1.50}Zn_{0.50}O_{3-\delta}$

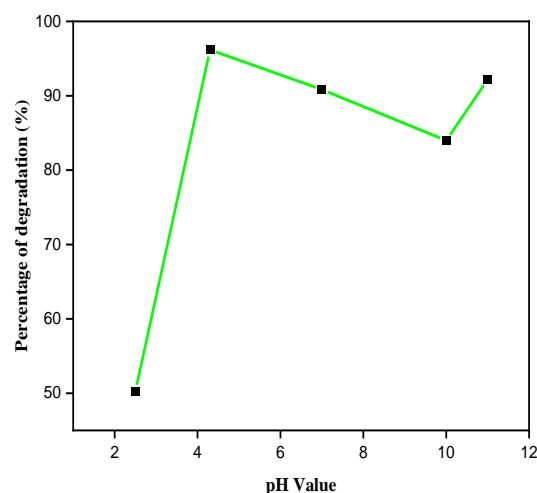


Fig. 16. Influence of pH on degradation efficiency

Also, similar degradation was noted at neutral pH and higher basicity [101]. The rate of degradation is less (50%) at lower acidic pH (2.5), which increases at higher acidic pH (4.3) reaching a percentage degradation of 96%. Hence, the percentage degradation at the pH range of 2.5, 4.3, 7, 10 and 11 was calculated as 50%, 96%, 90%, 83% and 92% respectively. It was observed that the lower degradation efficiency of the photocatalyst at pH of 2.5 can be attributed to the higher proton concentration in the lower acidic medium that consequently inhibits the dye degradation [79]. It was reported that, at a higher pH value, the RhB dye gets deprotonated [76] and such higher basic pH might enhance the generation of $\bullet\text{OH}$ radicals resulting in increased photodegradation through $\bullet\text{OH}$ radical oxidation mechanism. Due to variations in the catalytic surface, pH is a key variable in photocatalytic processes [102]. These changes can alter the pace at which the target molecule degrades. The charge on the catalyst surface is positive at pH levels below pH pzc and negative at pH levels above pH pzc. This thus alters the degree of dye adsorption on the catalyst surface. Since MB and RhB are in cationic configurations, pH values greater than pH_{pzc} are preferred for their adsorption [103]. According to the data, the photocatalyst showed improved adsorption characteristics and, consequently, better photocatalytic activity at intermediate pH values. The maximum photocatalytic rate was also noted in the starting solution pH of 4.3. The ideal pH for the photodecolorization of the mixture in the following experiments was determined to be pH 4.3. Finally, pH influences the degradation capacity at higher acidic, basic and neutral as well. The increased degradation at acidic pH is explained by an increase in the production of hydroxyl radicals [104], whereas, at basic pH, the

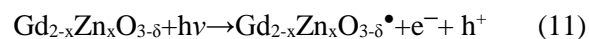
hydroxide ions involve in dye degradation until a certain range. Beyond pH=11, the hydroxide ions recombine with the photocatalysts forming their hydroxides. So an increase in pH also increases the effectiveness of decolorization. As evidenced by the findings, removal effectiveness declines above pH 9. It was discovered that two processes could result in the deactivation of $\bullet\text{OH}$ at high concentrations of OH. First, the reaction between $\bullet\text{OH}$ and $\bullet\text{OH}$ produced the H_2O_2 radicals. Compared to $\bullet\text{OH}$, these radicals have extremely little reactivity with organic color. Second, due to the quantity of $\bullet\text{OH}$ radicals, radical-radical interactions occur at higher pH levels. The literature contains reports of this response. In general, it has been documented that $\bullet\text{OH}$ deactivates at high pH levels. The dissociation of the dye molecules and the production of hydroxyl radicals are thus also impacted by pH, in addition to the catalyst's surface characteristics [104]. Therefore, the photocatalytic activity tends to change based on the pH levels as reported in the literature [105].

3.7.4. Proposed mechanism of photocatalysis

The efficiency of photocatalytic degradation of semiconductor oxides under UV light irradiation is related to the electronic band structure of the semi-conductor. On irradiation with a UV light source, the 4f level of lanthanide ions has a significant role in interfacial charge transfer and also in the elimination of electron-hole recombination for lanthanide doped sample. Lanthanide ions can act as an effective electron scavenger to trap the electrons in the conduction band of TiO_2 . When Ti^{4+} ions are substituted by lanthanide ions, more hydroxide ions get absorbed on the surface due to charge imbalance. These hydroxide ions act as hole traps that also inhibit electron-hole recombination [106]. Interfacial charge transfer should be a rate-determining step for photocatalytic reaction [107]. Similarly, in Gd^{3+} ions, abundant oxygen vacancies and surface defects are created which are actively involved in electron trapping and pollutant adsorption [108] thereby the recombination of electron-hole pairs is delayed effectively. The photocatalytic mechanism can be illustrated as follows:

In the mechanism of photocatalysis, the photocatalyst is irradiated with energy greater than or equal to its band gap energy to generate electron and hole pairs. The doping of Zn on Gd_2O_3 nanoparticles enhances the photocatalytic degradation of the dye. Two processes occur at the same time. Firstly, the electrons are ejected from the VB of $\text{Gd}_{2-x}\text{Zn}_x\text{O}_{3-\delta}$ which gets promoted to CB of $\text{Gd}_{2-x}\text{Zn}_x\text{O}_{3-\delta}$ particles by UV light irradiation. Secondly, the electrons are also promoted to the CB of Zn dopant from its VB due to the absorption of UV

radiation. At the same time, the electrons promoted to CB of Gd_2O_3 are promoted to the electrons/holes of the dopant through surface resonance effect. These electron-hole pairs migrate onto the surface of the photocatalyst where they interact with the dye (pollutant), finally resulting in degradation (Equations 11 to 14). In short, when the Gd_2O_3 and Zn doped Gd_2O_3 catalysts were illuminated by light, holes in the VB will be produced as the electrons in the VB and they got powered and bounced to the CB. These opened holes are treated with the encompassing H_2O and released as receptive hydroxyl radicals ($\bullet OH$). Also, the highly receptive oxygen free radicals ($O_2^{\bullet -}$) are produced when the formed electrons (e^-) react with the atmospheric oxygen molecules (O_2). These reactive species are responsible for complete RhB removal.



Thus, in presence of UV light source, the decolourisation is due to the conversion of the organic RhB dye carbons to CO_2 . The photocatalyst involves in the breakdown of the complex dye molecule into simpler and smaller molecules like CO_2 and H_2O . The photocatalytic reaction follows pseudo first order reaction kinetics as given by Langmuir – Hinshelwood kinetic model [109-110].

3.7.5 Scavenger Test- Identification of active species by in situ capture experiments

Photodegradation mechanism involves the generation of radicals like hydroxyl ($\bullet OH$), superoxide ($O_2^{\bullet -}$), electrons (e^-) and holes (h^+) during the irradiation process. The photocatalytic degradation pathway was examined for the best photocatalyst sample. It was discovered that the reactive oxidant species may be to blame for the decrease in the degradation rate. Reactive oxidative species such superoxide radical anions ($O_2^{\bullet -}$), hydroxyl radicals ($\bullet OH$), holes (h^+), and electrons were used to study the reaction mechanism (e^-). Using the hole-capturer EDTA-2Na, studies were conducted to establish the major reactive oxidative species responsible for the degradation of the RhB dye. Additionally, the O_2 and $\bullet OH$ scavengers typically utilized are p-benzoquinone and isopropyl alcohol (IPA), but the electron scavenger used in this study was DMSO [21]. A comparative study is made between the degradation curves of Zn doped Gd_2O_3 nanoparticles without the addition of scavengers and those which

involve the addition of quenchers to the initial solution by maintaining the experimental conditions identical. The fluctuation of C/C_0 of RhB as a function of the amount of time exposed to radiation both before and after scavengers was added to the photocatalytic system is shown in **Fig. 17**. After the scavengers were added to the photocatalytic system, the fluctuation of C/C_0 of the dyes was used to determine the involvement of the active species.

In presence of p-benzophenone (5 mg in 50 ml of Rh B solution), the transformation of the dye is completely suppressed suggesting that $O_2^{\bullet -}$ radical anions impart a major role in degradation pathway. Results indicate that, with addition of p-benzophenone (5 mg in 50 mL of Rh B solution), there was major reduction in degradation efficiency to 6%, under UV light irradiation [73]. Besides, on the introduction of IPA, there was a significant decrease in the degradation efficiency from 82% to 29% which clearly suggested that the $\bullet OH$ radical also has a vital role in the reaction pathway [111].

The addition of EDTA and DMSO to the mix accelerated the degradation of the RhB. As a result, the main species for the degradation reaction in Rh B are the radicals $\bullet OH$ and $O_2^{\bullet -}$. According to reports, when p-benzophenone was added to the photocatalytic system, a significant amount of $O_2^{\bullet -}$ was produced when the Zn- Gd_2O_3 ($Gd_{1.50}Zn_{0.50}O_{3-}$) photocatalyst was exposed to UV light. Furthermore, the electrons in the valence band go into the conduction band and create electron-hole pairs. [112]. The photocatalytic reaction's effectiveness has been decreased as a result of the surface recombination that allowed the excited electrons to also mix with holes. The addition of EDTA as a scavenger to collect holes prevented the recombination of electrons and holes in the system. As more electrons moved to the photocatalyst's surface, they reacted with O_2 to form $O_2^{\bullet -}$, which could speed up the RhB dye's decomposition. [113].

3.7.6 HPLC chromatographic analysis

Using a C18 analytical column to separate the substrate from the reaction products, HPLC chromatographic analysis was used to study the photooxidation reaction of RhB as a function of time. Analyzing the reaction products produced during the photo oxidation process can help you fully understand the reaction process. When exposed to UV light, the substrate dye RhB, which has four N-ethyl groups on either side of the xanthene ring, is quite stable in an aqueous solution. A calibration curve was used to ascertain how much RhB was used during the photodegradation process. **Fig.18 a**

and **b** show the typical HPLC chromatograms recorded for RhB dye before and after 80 min degradation respectively. The RhB chromatogram of **Fig. 18b** shows the highest peak with retention time, *t_R*, of 21.140 min with an area corresponding to 51.865%. Since the peak intensity of HPLC chromatograms is reduced from

93.55% to 54.48%, it is confirmed that the degradation occurs in the sample because of photocatalysis.

Fig. 19 shows the HPLC-MS analysis of the degraded RhB sample after 80 minutes. From the data, it was found that the degradation products have the *m/z* values of 329.25 and 478.55 corresponding to the removal of diethyl amine moiety and residual RhB in the analyte.

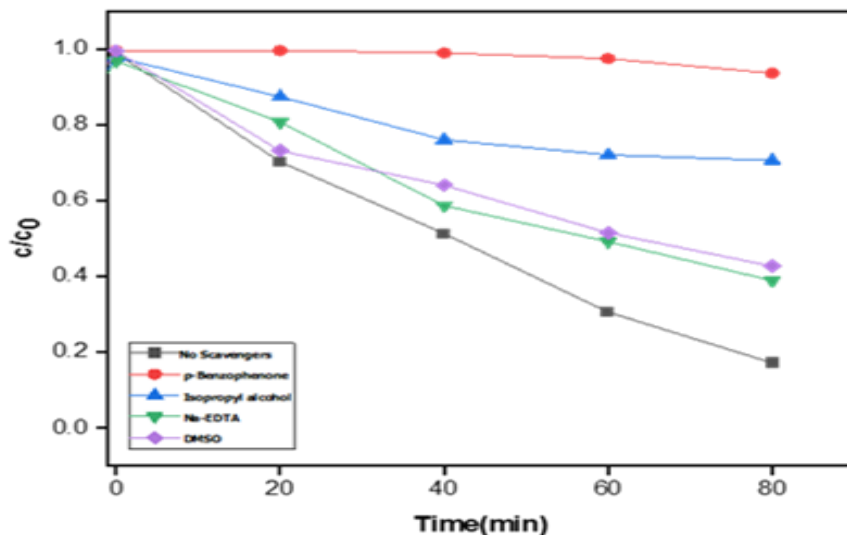


Fig. 17. Photocatalytic degradation of RhB by $Gd_{1.50}Zn_{0.50}O_{3-\delta}$ under UV light irradiation in the presence of scavengers

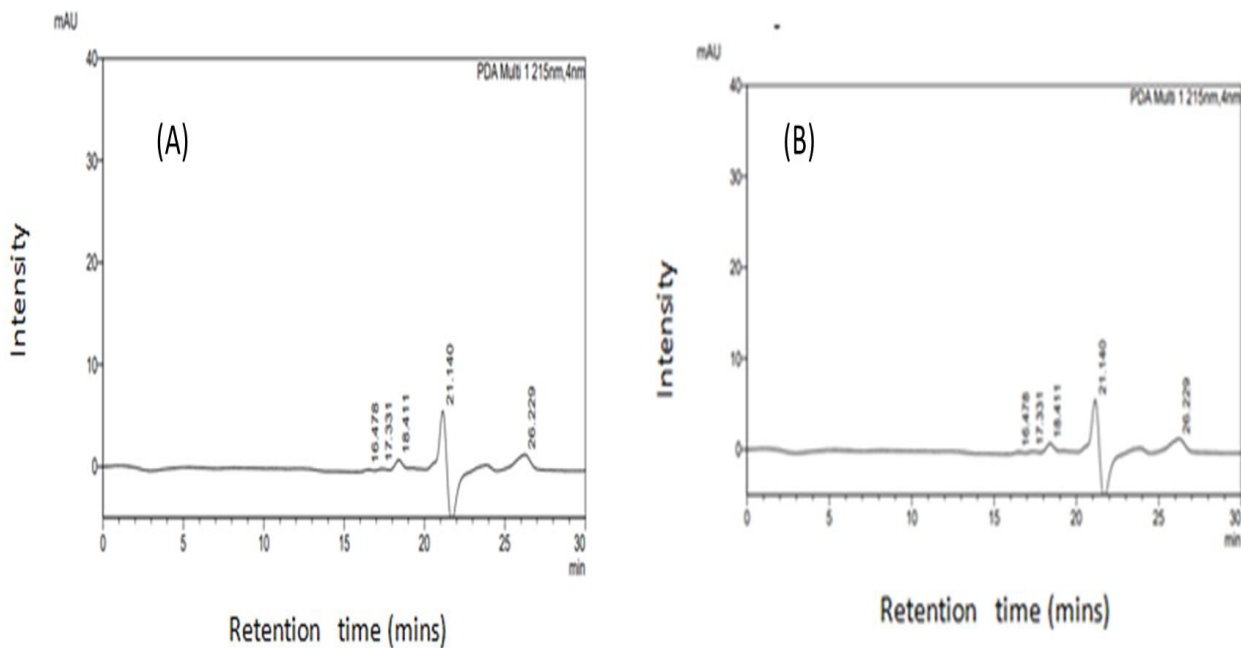


Fig. 18. Typical HPLC chromatograms recorded for RhB A) Before degradation, B) After 80 minutes degradation

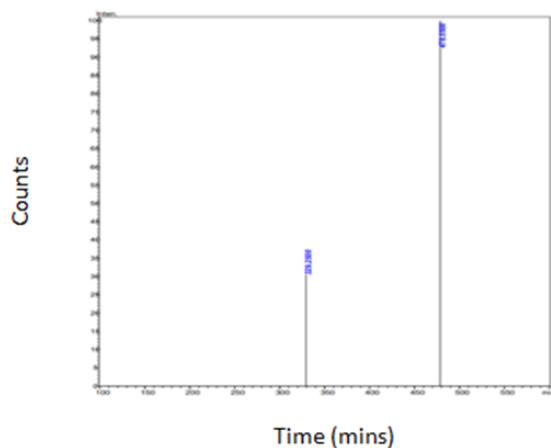


Fig. 19. HPLC-MS analysis of the degraded RhB sample after 80 minutes

4. Conclusions

In this research article, pure Gd_2O_3 and zinc doped Gd_2O_3 nanoparticles were synthesized by a simple chemical precipitation method and characterized by XRD, FTIR, SEM, EDX and UV analysis. The outcomes of our research highlight the photocatalytic activity of the produced photocatalysts in the decolorization of an aqueous RhB dye under UV light irradiation. The production of electron-hole pairs assisted the photocatalyst function. The OH ions in the aqueous RhB solution were converted into $\bullet OH$ radicals by holes with a high capacity for oxidation. Hydroxide ions and oxygen were coupled with valence band holes and conduction band electrons to form $OH\bullet$ and $O_2^{\bullet-}$. The dye molecules in RhB may be oxidized by the OH and O_2 radicals. In addition, a scavenger test also confirmed that the $OH\bullet$ and $O_2^{\bullet-}$ radicals have the major role in the degradation pathway of RhB. It was noted that when the adsorption of the dye molecules increases, the rate of photodegradation also increases. From the experimental results of the repetitive photocatalytic study, it was observed that $Gd_{1.50}Zn_{0.50}O_{3-\delta}$ photocatalyst showed outstanding photodegradation efficiency for RhB dye and thus seems to be an excellent reusable photocatalyst for the degradation of toxic organic pollutants from water with UV light irradiation. Therefore, these nanoparticles serve as potential photocatalysts in the degradation of dyes.

Acknowledgements

The Karunya Institute of Technology and Sciences (KITS), which has supported research on nanomaterials chemistry in the Department of Applied Chemistry, is acknowledged by the authors. TLV expresses gratitude

to KITS for providing the research facilities required to complete this project.

Disclosure statement

No potential conflict of interest was reported by the author.

References

- [1] R.L. Perez, G.M. Escandar, *Sustain. Chem. and Pharm.* 4 (2016) 1-12.
- [2] M. Rahsepar, M. Pakshir, Y. Piao, H. Kim, *Electrochim. Acta* 71 (2012) 246–251.
- [3] L. Li, Z. Lou, G. Shen, *ACS Appl. Mater. Interfaces*, 7 (2015) 23507– 23514.
- [4] M.K.M. Lane, J.B. Zimmerman, *Green Chem.* 21 (2019) 3769-3781.
- [5] S.Senobari, A.Nezamzadeh-Ejehieh, *Spectrochim.Acta A Mol.Biomol.* 196 (2018) 334 – 343.
- [6] M. Mittal, M. Sharma, O.P.Pandey, *Sol. Energy* 110 (2014) 386-397.
- [7] C. Wang, C. Shao, Y. Liu, X. Li, *Inorg. Chem.* 48 (2009) 1105-1113.
- [8] A.A. Khodja, T. Sehili, J.F. Pilichowski, P. Boule, *J. Photochem. Photobiol. A* 141 (2001) 231-239.
- [9] B. Cao, W. Cai, *J. Phys. Chem. C* 112 (2008) 680-685.
- [10] K. Atrak, A. Ramazani, S.T. Fardood, *J. Mater. Sci.: Mater Electron.* 29 (2018) 8347-8353.
- [11] M. Zhang, M. Wille, R. Rder, S. Heedt, L. Huang, Z. Zhu, S. Geburt, D. Grtzmacher, T. Schpers, C. Ronning, J.G. Lu, *Nano Lett.* 14 (2014) 518–523.
- [12] S. T. Fardood, R. Forootan, F. Moradnia, Z. Afshari, A. Ramazani, *Mater. Res. Express* 7 (2020) 015086.
- [13] A. Nezamzadeh-Ejehieh, E. Shahriari, *J. Ind. Eng. Chem.* 20 (2014) 2719-2726.
- [14] K. L. Seneviratne, I. Munaweera, S. E. Peiris, C. N. Peiris, N. Kottegoda, *Iran.J.Catal.* 11 (2021) 217 – 245.
- [15] L. Wang, J. Li, Y. Wang, L. Zhao, *J. Hazard. Mater.* 196 (2011) 342–349.
- [16] A.W. Xu, Y. Gao, H.Q. Liu, *J. Catal.* 207 (2002) 151-157.
- [17] Y.H. Zhang, H.L. Xu, Y.X. Xu, H.X. Zhang, Y.G. Wang, *J. Photochem. Photobiol. A* 170 (2005) 279–285.
- [18] H.Derikvandi, A.Nezamzadeh-Ejehieh, *J. Photochem. Photobiol. A: Chem.* 348 (2017) 68–78.

- [19] A.Yousefi, A.Nezamzadeh-Ejhih, Iran. J. Catal. 11 (2021) 247 – 259.
- [20] S. Jeon, J.-W. Ko, W.-B. Ko, Catalysts 11 (2021) 742.
- [21] S. Dhanalakshmi, P. Senthil Kumar, S. Karuthapandian, V. Muthuraj, N. Prithivikumaran, J. Mater. Sci. Mater. Electron. 30 (2019) 3744 – 3752.
- [22] D. Wu, C. Li, D. Zhang, L. Wang, X. Zhang, Z. Shi, Q. Lin, J. Rare Earths 37 (2019) 845-852.
- [23] M.I. Ghouri, E. Ahmed, N.R. Khalid, M. Ahmad, M. Ramzan, A. Shakoor, N.A. Niaz, J. Ovonic Res. 10 (2014) 89-100.
- [24] Y.B. Losovyj, D. Wooten, J.C. Santana, J.M. An, K.D. Belashchenko, N. Lozova, J. Petrosky, A. Sokolov, J. Tang, W. Wang, N. Arulsamy, P.A. Dowben, J. Phys.: Condens. Matter 21 (2009) 045602.
- [25] H. Guo, X. Yang, T. Xiao, W. Zhang, L. Lou, J. Mugnier, Appl. Surf. Sci. 230 (2004) 215-221.
- [26] A. Barrera, F. Tzompantzi, J.C. Molina, J.E. Casillas, R.P. Hernandez, S.U. Godinez, C. Velasquez, J.A. Alatorref, RSC Adv. 8 (2018) 3108 – 3119.
- [27] N. Saafie, M. F. R. Samsudin, S. Sufian, and R. M. Ramli, AIP. Conf. Proc. 2124 (2019) 020019-1–020019-10.
- [28] A. Ali, H. Zafar, M. Zia, I. U. Haq, A. R. Phull, J. S. Ali, A. Hussain, Nanotechnol. Sci. Appl. 9 (2016) 49 – 67.
- [29] J. Zhang, W. Wu, S. Yan, G. Chu, S. Zhao, X. Wang, C. Li, Appl. Surf. Sci. 344 (2015) 249 – 256.
- [30] R.M. Mohamed, I.A. Mkhaliid, E.S. Baeissa, M.A. Al-Rayyani, J. Nanotechnol. (2012) 329082.
- [31] D. Raiser, J.P. Deville, Spectrosc. Relat Phenom. 57 (1991) 91-97.
- [32] R.O. Yathisha, Y.A. Nayaka, J. Matter Sci. 53 (2018) 678–691.
- [33] K. Sujatha, T. Seethalakshmi, A.P. Sudha, O.L. Shanmugasundaram, Nano-Struct. Nano-Objects, 18 (2019) 100305.
- [34] S.F. Shayesteh, A. A. Dizgah, Pramana – J. Phys. 81 (2013) 319-330.
- [35] M. Pal, U. Pal, J.M.G.Y. Jiménez, F.P. Rodríguez, Nanoscale Res. Lett. 7 (2012) 1.
- [36] C. Rajashree, A.R. Balu, V.S. Nagarethinam, Surf Eng. 31 (2015) 316- 321.
- [37] G. K. Das, B.C. Heng, S. C. Ng, T. White, J.S.C. Loo, L. D’Silva, P. Padmanabhan, K. K. Bhakoo, S. Tamil Selvan, T.T.Y. Tan, Langmuir 26 (2010) 8959 – 8695.
- [38] V. Bedekar, D. P. Dutta, M. Mohapatra, S. V. Godbole, R. Ghildiyal, A. K. Tyagi, Nanotech. 20 (2009) 125707.
- [39] S. T. Fardood, F. Moradnia, S. Moradi, R. Forootan, F. Y. Zare, M. Heidari, Nanochem. Res. 4 (2019) 140-147.
- [40] T. F. Saeid, R. Ali, J.S. Woo, J. Appl. Chem. Res. 12 (2018) 8-15.
- [41] A. I. Y. Tok, F. Y. C. Boey, Z. Dong, X.L. Sun, J. Mater. Process. Technol. 190 (2007) 217-222.
- [42] R.K. Tamrakar, D. P. Bisen, K. Upadhyay, Lumin. 30 (2015) 812-817.
- [43] V. Mote, Y. Purushotham, B. Dole, J. Theor. Appl. Phys. 6 (6012) 6.
- [44] M. Balakrishnan, R. John, Iran. J. Catal. 10 (2020) 1-16.
- [45] S. Ghattavi, A. Nezamzadeh-Ejhih, Compos. B. Eng. 183 (2020) 107712.
- [46] T. Seyedi-Chokanlou, S. Aghabeygi, N. Molahasani, F. Abrinaei, Iran. J. Catal. 11 (2021) 49-58.
- [47] R. K. Tamrakar, D.P. Bisen, K. Upadhyay, N. Bramhe, J. Lumin. Appl. 1 (2014) 23-29.
- [48] R. K. Tamarakar, D.P. Bisen, C.S. Robinson, I.P. Sahu, N. Brahme, Ind. J. Mater. Sci. 396147 (2014) 1-7.
- [49] T. Yousefi, M.T. Mostaeidi, M. Ghasemi, A. Ghadirifar, Rare Metals 34 (2015) 540-545.
- [50] M. Sangmanee, S. Maensiri, App. Phys. A 97 (2009) 167-177.
- [51] N. Dhananjaya, H. Nagabhushana, B.M. Nagabhushana, B. Rudraswamy, S. C. Sharma, D. V. Sunitha, C. Shivakumara, R.P.S. Chakradhar, Spectrochim. Acta A Mol. Biomol. 96 (2012) 532-540.
- [52] V.A.M. Brabers, Phys. Status Solidi. 33 (1969) 563-572.
- [53] E. Moncada, R. Quijada, J. Retuert, Nanotech. 18 (2007) 335606.
- [54] H.E. Rassy, A.C. Pierre, J. Non-Cryst. Sol. 351 (2005) 1603-1610.
- [55] S. Esposito, M. Turco, G. Ramis, G. Bagnasco, P. Pernice, C. Pagliuca, M. Bevilacqua, A. Aronne. J. Solid State Chem. 180 (2007) 3341-3350.
- [56] R. S. Dubey, Y.B.R.D. Rajesh, M.A. More, Mater. Today: Proc. 2 (2015) 3575–3579.
- [57] P. Sharma, S.C. Brown, G. Walter, S. Santra, B. Moudgil, Adv. Colloid Interface 123–126 (2006) 471-485.
- [58] V. Parthasarathi, G. Thilagavathi, Int. J. Pharm. Pharm. Sci. 3 (2011) 392-398.

- [59] V. Srivastava, D. Gusain, Y.C. Sharma, *Ceram. Int.* 39 (2013) 9803-9808.
- [60] G. Xiong, U. Pal, J.G. Serrano, K.B. Ucer, R.T. Williams, *Phys. Stat. Sol. (C)* 3 (2006) 3577 - 3581.
- [61] A. Azam, F. Ahmed, N. Arshi, M. Chaman, A.H. Naqvi, *International Journal of Theoretical and Applied Sciences* 1 (2009) 12-14.
- [62] R. Wahab, Y.S. Kim, H.S. Shin, *Mater. Trans.* 50 (2009) 2092-2097.
- [63] R.M. Alwan, Q.A. Kadhim, K.M. Sahan, R.A. Ali, R. J. Mahdi, N.A. Kassim, A. N. Jassim, *Nanoscience and Nanotechnology* 5 (2015) 1-6.
- [64] A.D. Liyanage, S.D. Perera, K. Tan, Y. Chabal, K.J. Balkus Jr., *ACS Catal.* 4 (2014) 577 - 584.
- [65] J. Zhang, X. Shen, Q. Zhang, J.P.Y. Maa, G. Qiao, *Cont. Shelf Res.* 174 (2019) 85-94.
- [66] B. Rudraswamy, N. Dhananjaya, *IOP Conf. Ser: Mater. Sci. Eng.* 40 (2012) 012034.
- [67] F.Moradnia, S. T.Fardood, A.Ramazani, V. K. Gupta, *J. Photochem. Photobiol. A* 392 (2020) 112433.
- [68] S. T.Fardood, F.Moradnia, A. H.Ghalaichi, S.Daneshpajooh, M.Heidari, *Nanochem. Res.* 5 (2020) 69-76.
- [69] J. Nouri, T. Khoshraresh, S. Khanahmadzadeh, A. Salehabadi, M. Enhessari, *Int. J. Nano Dimens.* 7 (2016) 15-24.
- [70] P. Makuła, M. Pacia, W. Macyk, *J. Phys. Chem. Lett.* 9 (2018) 6814-6817.
- [71] G. Y. Adachi, N. Imanaka, *Chem. Rev.* 98 (1998)1479 - 1514.
- [72] Y.-H. Lin, C.-H. Weng, J.-H. Tzeng, Y.-T. Lin, *Int.J.Photoenergy* (2016) 3058429.
- [73] D. Neena, K.K. Kondamareddy, H. Bin, D. Lu, P. Kumar, R.K. Dwivedi, V.O. Pelenovich, X.Z. Zhao, W. Gao, D. Fu, *Sci. Rep.* 8 (2018)10691.
- [74] S. Paul, P. Chetri, B. Choudhury, G. A. Ahmed, A. Choudhury. *J. Colloid Interface Sci.* 439 (2015) 54-61.
- [75] S. Jeon, J.W. Ko, W.B. Ko, *Catalysts* 11 (2021) 742.
- [76] S. Dong, K. Xu, J. Liu, H. Cui, *Physica B* 406 (2011) 3609 - 3612.
- [77] A. Yousef, N.A.M. Barakat, T. Amna, A.R. Unnithan, S.S.A. Deyab, H.Y. Kim, *J. Lumin.* 132 (2012) 1668 -1677.
- [78] T.H. Le, A.T. Bui, T.K. Le, *Powder Technol.* 268 (2014) 173-176.
- [79] K.M. Reza, A.S.W. Kurny, F. Gulshan, *Appl. Water Sci.* 7 (2017) 1569-1578.
- [80] M. Saquib, M. Muneer, *Dyes Pigm.* 56 (2003) 37-49.
- [81] E.Abdelkader, L.Nadjia, B. Ahmed, *J. Chem. Eng. Process Technol.* 2 (2011) 1000106 (1-9).
- [82] J.Z. Bloh, *Front Chem.* 7 (2019) 128.
- [83] D.F. Ollis, *Front Chem.* 6 (2018) 378.
- [84] C. Casado, J. Marugán, R. Timmers, M. Muñoz, R. van Grieken, *Chem. Eng J.* 310 (2017) 368-380.
- [85] A. Tolosana-Moranchel, C. Pecharromán, M. Faraldos, A. Bahamonde, *Chem. Eng. J.* 403 (2021) 126186.
- [86] A. Tolosana-Moranchel, J.A. Casas, J. Carbajo, M. Faraldos, A. Bahamonde, *Appl. Catal. B Environ.* 200 (2017) 164-173.
- [87] N.Raeesi-Kheriabadi, A.Nezamzadeh-Ejhieh, *Int.J.Hydrog.Energy* 45 (2020) 33381-33395.
- [88] A. Sobhani-Nasab, M. Eghbali-Arani, Seyed M. Hosseinpour-Mashkani, F. Ahmadi, M. Rahimi-Nasrabadi, V.Ameri, *Iran.J.Catal.* 10 (2020) 91-99.
- [89] B. Manikandan, K. R. Murali, R. John, *Iran.J.Catal.* 11 (2021) 1.
- [90] S.Ghattavi, A. Nezamzadeh-Ejhieh, *Int.J.Hydrog.Energy* 45 (2020) 24636-24656.
- [91] N.Omrani, A. Nezamzadeh-Ejhieh, *Sep.Purif.Technol.* 235 (2020) 116228.
- [92] S.Ghattavi, A. Nezamzadeh-Ejhieh, *Compos.B.Eng.* 183 (2020) 107712.
- [93] M.Mehrali-Afjani, A.Nezamzadeh-Ejhieh, H.Aghaei, *Chem. Phys. Lett.* 759 (2020) 137873.
- [94] A.Yousefi, A.Nezamzadeh-Ejhieh, *Iran.J.Catal.* 11 (2021) 247 - 259.
- [95] S.Salmanderis, A.Nezamzadeh-Ejhieh, *Desalin.Water Treat.* 197 (2020) 200-212.
- [96] P. Jantawasu, T. Sreethawong, S. Chavadej, *Chem. Eng J.* 155 (2009) 223-233.
- [97] U.G. Akpan, B.H. Hameed, *J. Hazard. Mater.* 170 (2009) 520-529.
- [98] R. Saleh, N.F. Djaja, *SuperlatticeMicrost.* 74 (2014) 217-233.
- [99] A.Pourtaheri, A.Nezamzadeh-Ejhieh, *Spectrochim.Acta A Mol.Biomol.* 137 (2015) 338-344.
- [100] M. G. Antoniou, D.D. Dionysiou, *Catal. Today* 124 (2007) 215- 223.
- [101] L. Rancano, M. J. Rivero, M.Á. Mueses, I. Ortiz, *Catalysts* 11 (2021) 48.
- [102] K. Byrappa, A.K. Subramani, S. Ananda, K.M. Lokanatharai, R. Dinesh, M. Yoshimura, *Bull. Mater.Sci.* 29 (2006) 433-438.

- [103] A. Nezamzadeh-Ejhi, M. Khorsandi, J. Hazard. Mater. 176 (2010) 629-637.
- [104] J. Xu, Y. Ao, D. Fu, C. Yuan, Colloids and Surfaces A: Physicochem. Eng. Aspects 334 (2009) 107-111.
- [105] M. Rezaei, A. Nezamzadeh-Ejhi, Int. J. Hydrog. Energy 45 (2020) 24749-24764.
- [106] H. Liu, X.Z. Li, Y.J. Leng, W.Z. Li, J. Phys. Chem. B 107 (2003) 8988-8996.
- [107] W. Li, R. Liang, A. Hu, Z. Huang, Y.N. Zhou, RSC Adv. 4 (2014) 36959-36966.
- [108] M. Madhukar Naik, H.S. Bhojya Naik, G. Nagaraju, M. Vinuth, K. Vinu, R. Viswanath, Nano-Struct. Nano-Objects 19 (2019) 100322.
- [109] S. Pan, X. Liu, New J. Chem. 36 (2012) 1781-1787.
- [110] A. Nezamzadeh-Ejhi, M. Karimi-Shamsabadi, Chem. Eng. Sci. 228 (2013) 631-641.
- [111] M. Sharma, A. Kumar, R. K. Gautam, M. Belwal, J. Nanosci. Nanotechnol. 18 (2018) 3532-3535.
- [112] T. Liu, L. Wang, X. Lu, J. Fan, X. Cai, B. Gao, R. Miao, J. Wang, Y. Lv, RSC Adv. 7 (2017) 12292.
- [113] M.S. Adly, Sh.M. El-Dafrawy, S.A. El-Hakam, J. Mater. Res. Technol. 8 (2019) 5610-5622.